Differential Regulation of ER Ca^{2+} Uptake and Release Rates Accounts for Multiple Modes of Ca^{2+}-induced Ca^{2+} Release

Meredith A. Albrecht, Stephen L. Colegrove, and David D. Friel

Department of Neurosciences, Case Western Reserve University, Cleveland, OH 44106

ABSTRACT The ER is a central element in Ca^{2+} signaling, both as a modulator of cytoplasmic Ca^{2+} concentration ($[Ca^{2+}]_i$) and as a locus of Ca^{2+}-regulated events. During surface membrane depolarization in excitable cells, the ER may either accumulate or release net Ca^{2+}, but the conditions of stimulation that determine which form of net Ca^{2+} transport occurs are not well understood. The direction of net ER Ca^{2+} transport depends on the relative rates of Ca^{2+} uptake and release via distinct pathways that are differentially regulated by Ca^{2+}, so we investigated these rates and their sensitivity to Ca^{2+} using sympathetic neurons as model cells. The rate of Ca^{2+} uptake by SERCAs (J_{SERCA}), measured as the t-BuBHQ-sensitive component of the total cytoplasmic Ca^{2+} flux, increased monotonically with $[Ca^{2+}]_i$. Measurement of the rate of Ca^{2+} release ($J_{Release}$) during t-BuBHQ-induced $[Ca^{2+}]_i$ transients made it possible to characterize the Ca^{2+} permeability of the ER ($\tilde{P}_{ER}$), describing the activity of all Ca^{2+}-permeable channels that contribute to passive ER Ca^{2+} release, including ryanodine-sensitive Ca^{2+} release channels (RyRs) that are responsible for CICR. Simulations based on experimentally determined descriptions of J_{SERCA}, $\tilde{P}_{ER}$, and of Ca^{2+} extrusion across the plasma membrane (J_{pm}) accounted for our previous finding that during weak depolarization, the ER accumulates Ca^{2+}, but at a rate that is attenuated by activation of a CICR pathway operating in parallel with SERCAs to regulate net ER Ca^{2+} transport. Caffeine greatly increased the $[Ca^{2+}]$ sensitivity of $\tilde{P}_{ER}$, accounting for the effects of caffeine on depolarization-evoked $[Ca^{2+}]_i$ elevations and caffeine-induced $[Ca^{2+}]_i$ oscillations. Extending the rate descriptions of J_{SERCA}, $\tilde{P}_{ER}$, and J_{pm} to higher $[Ca^{2+}]_i$ levels shows how the interplay between Ca^{2+} transport systems with different Ca^{2+} sensitivities accounts for the different modes of CICR over different ranges of $[Ca^{2+}]_i$ during stimulation.

KEY WORDS: CICR • ER • ryanodine receptors • SERCA • sympathetic neurons

INTRODUCTION

The ER is an important component in Ca^{2+} signaling in virtually all nonmuscle cells (Pozzan et al., 1994; Clapham, 1995; Berridge, 1998; Meldolesi and Pozzan, 1998). Net Ca^{2+} transport by the ER is critical for regulating intraluminal Ca^{2+} concentration ($[Ca^{2+}]_{ER}$), as well as for modulating the dynamics of cytoplasmic free Ca concentration ($[Ca^{2+}]_i$) during and after stimulation. As a result, Ca^{2+} transport by this organelle is expected to influence the activity of Ca^{2+}-sensitive processes within the ER and the cytoplasm, as well as in organelles such as mitochondria and the nucleus that undergo secondary changes in intraluminal Ca^{2+} concentration in response to evoked changes in $[Ca^{2+}]_i$ (Gerasimenko et al., 1996; Babcock and Hille, 1998).

In neurons, the role that the ER plays in modulating depolarization-induced $[Ca^{2+}]_i$ elevations is complicated, since this organelle may act as either a Ca^{2+} source or sink, in some cases even in the same cell type (Friel and Tsien, 1992a; Garaschuk et al., 1997; Toescu, 1998; for review see Simpson et al., 1995; Rose and Konnerth, 2001). These distinct forms of net ER Ca^{2+} transport are expected to have very different functional effects on the activity of intraluminal Ca^{2+} binding proteins (Corbett and Michalak, 2000). Nevertheless, the conditions of stimulation that determine which form of transport occurs are incompletely understood. The direction and rate of net ER Ca^{2+} transport depend on the relative rates of Ca^{2+} uptake and release via distinct transport pathways. Ca^{2+} uptake is regulated by sarco(endo)plasmic reticulum Ca ATPases (SERCAs;* East, 2000), whereas passive Ca^{2+} release is regulated by Ca^{2+} release channels that open in response to elevations in $[Ca^{2+}]_i$ and contribute to Ca^{2+}-induced Ca^{2+} release (CICR; Bezprozvanny et al., 1991; Ehrlich, 1995; for reviews see Kuba, 1994; Verkhratsky and Shmigol, 1996; Usachev and Thayer, 1999). If the rate of Ca^{2+} uptake exceeds the rate of release, the ER acts as a Ca^{2+} sink and slows depolarization-evoked $[Ca^{2+}]_i$ elevations. If release is faster than uptake, it acts as a

Address correspondence to David Friel, Ph.D., Department of Neurosciences, Case Western Reserve University, 10900 Euclid Avenue, Cleveland, OH 44106. Fax: (216) 368-4650; E-mail: ddf2@po.cwru.edu

*Abbreviations used in this paper: [Ca], total Ca concentration; FCCP, carbonyl cyanide p-(trifluoromethoxy)phenylhydrazone; $InsP_3R$, D-*myo*-inositol 1,4,5-trisphosphate receptor; SERCA, sarco(endo)plasmic reticulum Ca ATPase; t-BuBHQ, 2,5-Di-(t-butyl)-1,4-hydroquinone; Tg, thapsigargin.

Ca^{2+} source, speeding and potentially amplifying these responses.

The main goal of the present study was to understand how differential regulation of ER Ca^{2+} uptake and release rates by Ca^{2+} determines the direction and rate of net ER Ca^{2+} transport during stimulation. Our previous work in sympathetic neurons showed that as evoked $[Ca^{2+}]_i$ elevations become larger, the ER undergoes a transition from a Ca^{2+} sink to a Ca^{2+} source (Albrecht et al., 2001; Hongpaisan et al., 2001). Specifically, it was found that if $[Ca^{2+}]_i$ is raised to less than or equal to ~350 nM by weak depolarization, the ER accumulates Ca^{2+}, whereas if global $[Ca^{2+}]_i$ is raised to 600–800 nM by stronger depolarization, there is little or no net ER Ca^{2+} transport. However, if $[Ca^{2+}]_i$ rises to higher levels during depolarization, for example, in outer cytoplasmic regions near sites of Ca^{2+} entry, or during inhibition of mitochondrial Ca^{2+} uptake, the ER releases net Ca^{2+}, presumably reflecting net CICR. We proposed a simple explanation for this transition: progressive $[Ca^{2+}]_i$-dependent activation of a ryanodine-sensitive CICR pathway that operates in parallel with SERCAs to regulate net ER Ca^{2+} transport. According to this idea, small $[Ca^{2+}]_i$ elevations stimulate Ca^{2+} uptake more effectively than Ca^{2+} release, leading to Ca^{2+} accumulation, whereas large $[Ca^{2+}]_i$ elevations stimulate release more effectively than uptake, leading to net Ca^{2+} release. We also presented indirect evidence that activation of the CICR pathway is influential even when $[Ca^{2+}]_i$ is low and the ER acts as a Ca^{2+} sink, causing the rate of ER Ca^{2+} accumulation to be reduced so that the ER becomes a less powerful buffer.

A quantitative model was presented, which showed that this idea is plausible (Albrecht et al., 2001). In terms of the model, differential regulation of ER Ca^{2+} uptake and release rates by Ca^{2+} is the key factor in determining when the ER acts as a Ca^{2+} source or sink. Moreover, we proposed that the relative rates of net ER Ca^{2+} transport and Ca^{2+} clearance by other pathways determine whether net Ca^{2+} release, if it occurs, can be regenerative.

In the present study, we test some of these ideas by characterizing the Ca^{2+} transport pathways responsible for ER Ca^{2+} uptake and release in sympathetic neurons. We sought to determine how Ca^{2+} transport by each pathway is regulated by Ca^{2+} when $[Ca^{2+}]_i$ is low and the ER acts as a Ca^{2+} sink. It was asked if quantitative differences in the Ca^{2+}-dependent regulation of Ca^{2+} uptake and release rates can account for Ca^{2+} accumulation at low $[Ca^{2+}]_i$ at a rate that is reduced by activation of a ryanodine-sensitive CICR pathway. We also sought to understand how $[Ca^{2+}]_i$-dependent regulation of ER Ca^{2+} uptake and release rates determines when the ER is a Ca^{2+} source or sink over a wider $[Ca^{2+}]_i$ range, and how net ER Ca^{2+} transport contributes to multiple modes of CICR.

MATERIALS AND METHODS

Cell Dissociation and Culture

Bullfrog sympathetic neurons were dissociated and placed in culture for up to 1 wk, as described previously (Colegrove et al., 2000a). All procedures conform to guidelines established by our Institutional Animal Care and Use Committee.

Cytoplasmic Calcium Measurements

To measure $[Ca^{2+}]_i$, cells were incubated with 3 μM fura-2 AM in normal Ringer's solution for 40 min at room temperature with gentle agitation followed by rinsing. The composition of normal Ringer's solution was the following (in mM): 128 NaCl, 2 KCl, 2 $CaCl_2$, 10 HEPES, and 10 glucose, pH adjusted to 7.3 with NaOH. Fura-2 AM was dispensed from a 1-mM stock solution in DMSO containing 25% (wt/wt) pluronic F127 (BASF Corporation). Cells were washed with normal Ringer's solution and placed on the stage of an inverted microscope (Diaphot TMD; Nikon) and superfused continuously (~5 ml/min). Recordings began ~20 min after washing away fura-2 AM, permitting de-esterification of the Ca^{2+} indicator. With this loading procedure, there is little compartmentalization of fura-2 (Albrecht et al., 2001). Solution changes (~200 ms) were made using a system of microcapillaries (20 μl; Drummond microcaps) mounted on a micromanipulator. Fluorescence measurements were performed as described in Colegrove et al. (2000a).

Ca^{2+} Flux Measurements

In this study, three different macroscopic Ca^{2+} fluxes were measured: (1) J_{SERCA}, the rate of Ca^{2+} uptake via SERCAs; (2) J_i, the total cytoplasmic Ca^{2+} flux when SERCAs are inhibited; and (3) J_{pm}, the rate of Ca^{2+} extrusion across the plasma membrane. One additional flux ($J_{Release}$) was calculated from the difference between two of the measured fluxes (J_i and J_{pm}). Finally, $J_{Release}$ and its integral were used to obtain information about intraluminal Ca^{2+} concentration and the Ca^{2+} permeability of the ER ($\tilde{P}_{ER}$).

Fluxes were measured using the following experimental protocols. To determine J_{SERCA}, cells were rapidly exposed to a saturating concentration (100 μM) of the SERCA inhibitor 2,5-Di-(t-butyl)-1,4-hydroquinone (t-BuBHQ), using the abrupt change in $d[Ca^{2+}]_i/dt$ after application of the inhibitor as a measure of the t-BuBHQ-sensitive component of the total cytoplasmic Ca^{2+} flux (see Fig. 2 A). To measure this change, lines were fit to the linear portions of the $[Ca^{2+}]_i$ record just before and after the perturbation, and J_{SERCA} was taken as the difference between the final and initial slopes. The total cytoplasmic Ca^{2+} flux (J_i) during t-BuBHQ-induced $[Ca^{2+}]_i$ transients (see Fig. 3, A and B) was calculated as the time derivative of $[Ca^{2+}]_i$ at each sample time t_i according to $([Ca^{2+}]_i(t_i + \Delta t/2) - [Ca^{2+}]_i(t_i - \Delta t/2))/\Delta t$, where Δt (400–500 ms) is twice the sampling interval. For the first and last sample points, the flux was estimated by computing the slope of a fitted line over the first and last sets of three sample points, respectively. The rate of Ca^{2+} extrusion across the plasma membrane (J_{pm}) was determined by measuring the total cytoplasmic Ca^{2+} flux during the $[Ca^{2+}]_i$ recovery after brief high K^+ depolarizations while cells were continuously exposed to t-BuBHQ, and to FCCP to inhibit mitochondrial Ca^{2+} uptake (see Fig. 3, A–C; Colegrove et al., 2000a). The rate of passive Ca^{2+} release from the ER ($J_{Release}$) during the t-BuBHQ-induced $[Ca^{2+}]_i$ transient was then taken as the difference between J_i and J_{pm} at corresponding times (Fig. 3 B). J_{pm} was determined at each point in time during the $[Ca^{2+}]_i$ transient based on the rate of Ca^{2+} extrusion during the recovery after depolarization at corresponding values of $[Ca^{2+}]_i$. This is justified by our previous finding that, in

sympathetic neurons, J_{pm} can be specified at each time by the magnitude of $[Ca^{2+}]_i$ at that time (Colegrove et al., 2000a). Before calculating $d[Ca^{2+}]_i/dt$, $[Ca^{2+}]_i$ measurements were smoothed with a binomial filter. Since measurements were acquired with regular sample intervals, J_i and J_{pm} were not always measured at identical values of $[Ca^{2+}]_i$, so to facilitate flux subtraction, linear interpolation was used to approximate each of the measured fluxes at equally spaced values of $[Ca^{2+}]_i$.

As shown in APPENDIX A, if Ca^{2+} binding to cytoplasmic buffers equilibrates rapidly compared with changes in $[Ca^{2+}]_i$, each measured Ca^{2+} flux can be interpreted as the rate of Ca^{2+} transport by the respective system (e.g., $\tilde{J}$ in nmol/s) divided by the product of the cytoplasmic volume (v_i) and a buffering factor (κ_i) that gives the change in total cytoplasmic Ca concentration accompanying small changes in $[Ca^{2+}]_i$ (Neher and Augustine, 1992; Tse et al., 1994; Neher, 1995; Colegrove et al., 2000a). While it was assumed that v_i is constant, κ_i was treated as a function of $[Ca^{2+}]_i$ (see next section). Thus, the measured fluxes are expected to show a composite $[Ca^{2+}]_i$ dependence that reflects Ca^{2+}-dependent regulation of the individual transport rates and the $[Ca^{2+}]_i$ dependence of κ_i.

To determine if the measured fluxes account for the time course of $[Ca^{2+}]_i$ after various experimental perturbations, quantitative descriptions of J_{pm}, J_{SERCA}, $\tilde{P}_{ER}$, and κ_i were used as the defining equations in the model described in APPENDIX B. Quantitative descriptions of the fluxes were of the form $\tilde{J}/(v_i\kappa_i)$, where $\tilde{J}$ is represented by a Hill-type equation, or in the case of J_{pm}, such an equation plus a leak, v_i is constant and κ_i is a known function of $[Ca^{2+}]_i$ (see next section). Parameters of these equations were estimated based on the flux versus $[Ca^{2+}]_i$ measurements. While mechanistically motivated, the equations used to describe the $[Ca^{2+}]_i$ dependence of transport by the different pathways should be regarded as empirical, since the $[Ca^{2+}]_i$ range over which measurements were made was not always broad enough to determine unique parameter sets. Nevertheless, as shown in RESULTS, given equations that accurately describe the $[Ca^{2+}]_i$ dependence of the measured fluxes, it is possible to account for $[Ca^{2+}]_i$ dynamics after various experimental perturbations. Given information about the $[Ca^{2+}]_i$ dependence of κ_i, it is also possible to make inferences about the $[Ca^{2+}]_i$ dependence of transport rates and $[Ca^{2+}]_i$ dynamics in cells without exogenous Ca^{2+} buffers, but this was not the focus of the present study.

To examine qualitative properties of CICR over a wider range of $[Ca^{2+}]_i$, continuous extensions of the descriptions for J_{pm}, J_{SERCA}, and $\tilde{P}_{ER}$, were used. In this case, there is uncertainty regarding quantitative features of the simulations (e.g., precise values of $[Ca^{2+}]_i$ thresholds for net CICR), but the qualitative features (e.g., the existence of thresholds and their order relationship) are expected to be reliable. Nevertheless, experimental characterization of the transport systems at higher $[Ca^{2+}]_i$ levels is an important goal of future experiments.

Cytoplasmic Ca^{2+} Buffering

To characterize the Ca^{2+} permeability of the ER, it was necessary to obtain information about the driving force favoring passive Ca^{2+} release during t-BuBHQ-induced $[Ca^{2+}]_i$ transients (APPENDIX A). Information about changes in intraluminal Ca^{2+} concentration was obtained by integrating $J_{Release}$ over time. However, since $J_{Release}$ is a flux per unit (effective) cytoplasmic volume (in $nmol/v_i\kappa_i/s$), conversion to a flux per unit (effective) intraluminal volume (in $nmol/v_{ER}\kappa_{ER}/s$) was required before integration. The appropriate flux was obtained after multiplying $J_{Release}$ by $(v_i\kappa_i/v_{ER}\kappa_{ER})$. It was assumed that (1) v_i/v_{ER} is constant, (2) κ_{ER} is constant, as would be expected if intraluminal Ca^{2+} buffers have low affinity for Ca^{2+}, and (3) that κ_i adjusts instantaneously to changes in total Ca concentration. Evaluation of κ_i and its $[Ca^{2+}]_i$ dependence required consideration of fura-2, since this Ca^{2+} indicator must contribute to cytoplasmic Ca^{2+} buffering in our experiments and binds Ca^{2+} with moderately high affinity ($K_{d,Fura\text{-}2} \sim 224$ nM). To evaluate this potential contribution to the $[Ca^{2+}]_i$ dependence of κ_i, the experiments illustrated in Fig. 1 were performed.

Fig. 1 (A and B) shows a representative voltage-sensitive Ca^{2+} current and associated $[Ca^{2+}]_i$ response elicited from a fura-2 AM–loaded sympathetic neuron by weak depolarization under voltage clamp (perforated patch conditions). Using standard methods (Albrecht et al., 2001), we measured the cytoplasmic buffering strength $\kappa_{i,basal}$ when $[Ca^{2+}]_i$ was at its resting level. By progressively reducing the fura-2 AM incubation time, it was possible to estimate the resting value of κ_i in native, unloaded cells, as well as the component of κ_i representing fura-2 in our experiments, where the incubation time was 40 min. As expected, κ_i is smaller if the incubation time is reduced (Fig. 1 C). The dependence of κ_i on loading time could be described empirically by a third-order polynomial function, and extrapolation to zero incubation time provides an estimate of the endogenous cytoplasmic Ca^{2+} buffering strength at rest ($\kappa_{i,Endog} \sim 25$). The strength of buffering ($\kappa_{i,Fura\text{-}2}$) by fura-2 at the 40-min time point then was calculated as $\kappa_{i,basal} - \kappa_{i,Endog} \sim 238$. Thus, under our experimental conditions, fura-2 represents the major cytoplasmic Ca^{2+} buffer at rest. This made it possible to describe explicitly the $[Ca^{2+}]_i$ dependence of κ_i in our experiments as follows (Fig. 1 D):

$$\begin{aligned}\kappa_i &= \kappa_{i,Endog} + \kappa_{i,Fura2} \\ &= \kappa_{i,Endog} + [\text{Fura-2}]K_{d,Fura2}/(K_{d,Fura2} + [Ca^{2+}]_i)^2.\end{aligned} \quad (1)$$

Given κ_i, $\kappa_{i,Endog}$, $K_{d,Fura2}$, and the mean resting $[Ca^{2+}]_i$ (Fig. 1, legend), Eq. 1 permits calculation of the average cytoplasmic fura-2 concentration ([Fura-2]) after a 40-min incubation, ~80 μM. Thus, assuming that $\kappa_{i,Endog}$ is constant, small elevations in $[Ca^{2+}]_i$ starting from initial values within the range 50–300 nM are associated with changes in total cytoplasmic Ca concentration between ~250× and 100× as large, with most of the Ca^{2+} being bound by fura-2. Based on these measurements and assumptions 1–3 above, $(v_i\kappa_i/v_{ER}\kappa_{ER})$ was treated as the product of a constant $(v_i/v_{ER}\kappa_{ER})$ and a $[Ca^{2+}]_i$-dependent term κ_i that could be described explicitly by the curve in Fig. 1 D. Note that this treats all cells as if they have identical cytoplasmic Ca^{2+} buffering properties; in the absence of single cell measurements of κ_i and its $[Ca^{2+}]_i$ dependence, this seems to be a reasonable simplifying assumption. As described in APPENDIX A, information about the $[Ca^{2+}]_i$ dependence of κ_i was used to convert $J_{Release}$ into a flux that could be integrated to give information about changes in intraluminal Ca^{2+} concentration during t-BuBHQ-induced $[Ca^{2+}]_i$ transients.

Inhibition of CICR

To inhibit CICR, cells were exposed to ryanodine (1 μM) and then transiently to caffeine (10 mM) in the continued presence of ryanodine. Under these conditions, caffeine elicits a transient rise in $[Ca^{2+}]_i$ like that observed in control cells, but unlike control cells, responsiveness to caffeine is not restored after caffeine is removed (Thayer et al., 1988). Caffeine opens RyRs by increasing their sensitivity to $[Ca^{2+}]_i$ (Rousseau et al., 1988), and ryanodine is thought to inhibit caffeine responsiveness by irreversibly modifying RyRs so that they are insensitive to Ca^{2+} (Rousseau et al., 1987) or have greatly increased Ca^{2+} sensitivity (Masumiya et al., 2001). Ryanodine was used in conjunction with caffeine because ryanodine preferentially interacts with the open channel, causing ryanodine-induced RyR modifications to be use-dependent.

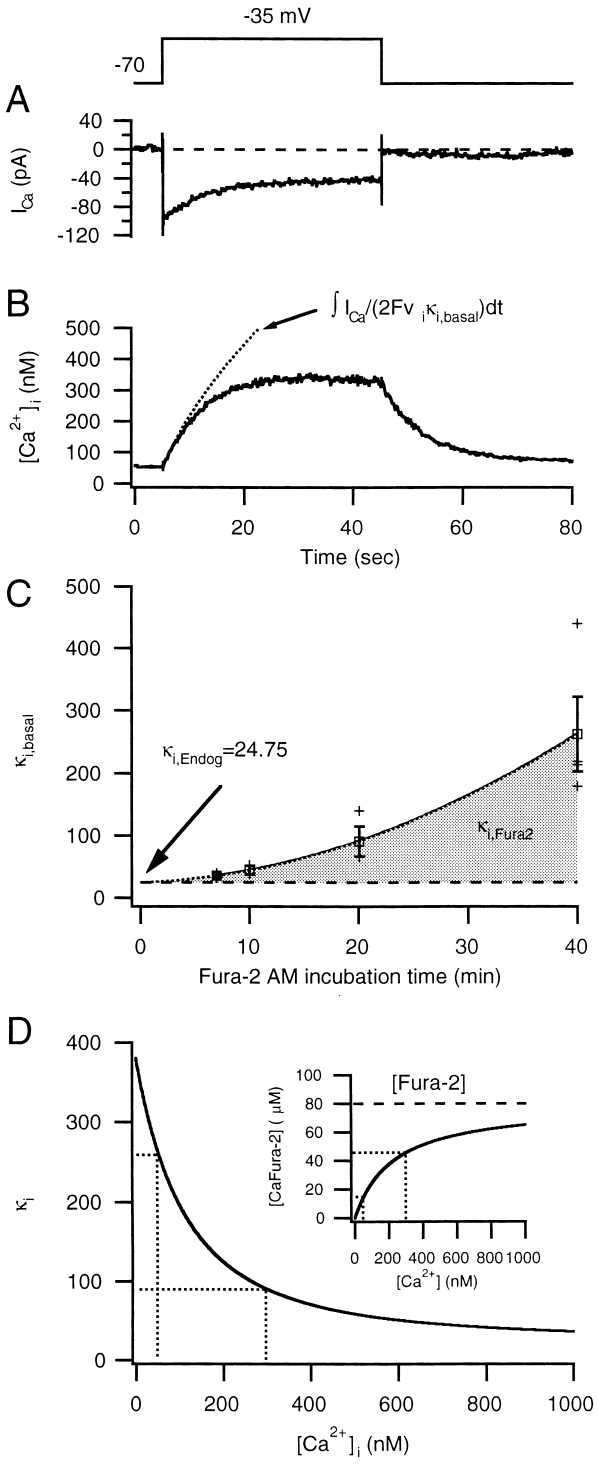

FIGURE 1. Characterization of cytoplasmic Ca^{2+} buffering. (A and B) Depolarization-evoked Ca^{2+} current (I_{Ca}) and $[Ca^{2+}]_i$ elevation elicited in a fura-2 AM–loaded sympathetic neuron under voltage clamp (perforated patch conditions). Dotted trace shows the calculated change in free Ca concentration expected for this Ca^{2+} current in the absence of other fluxes, calculated by integrating $I_{Ca}/2Fv_i\kappa_{i,Basal}$, where F is the Faraday constant, v_i is the cytoplasmic volume, and $\kappa_{i,basal}$ is the cytoplasmic buffering factor determined as in Albrecht et al. (2001). (C) Determination of endogenous Ca^{2+} buffering strength. Cells were incubated with 3 μM fura-2 AM for different periods of time to systematically vary exogenous Ca^{2+} buffering strength. Mean $\kappa_{i,basal}$ values were fit with a third-order polynomial that was extrapolated to zero incubation time, giving an estimated endogenous buffering strength ($\kappa_{i,Endog}$) of 24.75. The shaded region describes Ca^{2+} buffering attributable to fura-2 for the different incubation times. Numbers of cells for each incubation time (in min) were as follows: 3 (7), 2 (10), 3 (20), and 4 (40). Crosses indicate single cell measurements and squares give mean values. (D) Calculated $[Ca^{2+}]_i$ dependence of κ_i in the case of a 40-min incubation period like that used in the present study. Dotted lines indicate κ_i when $[Ca^{2+}]_i$ = 50 and 300 nM. Inset shows predicted Ca^{2+} binding by fura-2 as a function of $[Ca^{2+}]_i$. The average fura-2 concentration ([Fura-2]) was determined by solving Eq. 1 under resting conditions ($[Ca^{2+}]_i$ = 49 ± 5.8 nM; N = 4) assuming that $K_{d,Fura-2}$ = 224 nM, giving [Fura-2] = 79.7 μM.

Data Analysis and Reagents

Population results are expressed as mean ± SEM, and statistical significance was assessed using *t* test. Fura-2 AM was obtained from Molecular Probes, ryanodine was obtained from RBI, and t-BuBHQ was purchased from Calbiochem. All other compounds were obtained from Sigma-Aldrich.

Simulations

Rate equations describing Ca^{2+} extrusion across the plasma membrane (Colegrove et al., 2000b) and Ca^{2+} uptake and release by the ER were incorporated into a system of differential equations (see APPENDIX B) that was solved numerically using a fourth-order Runge-Kutta routine (Boyce and DiPrima, 1969) written in Igor Pro (Wavemetrics, Inc.). Step size was 50 ms; further reductions in step size did not noticeably alter the results.

RESULTS

In the following, we will describe measurements of the rate of ER Ca^{2+} uptake by SERCAs (J_{SERCA}), illustrating how it varies with $[Ca^{2+}]_i$. We will describe measurements of the rate of passive Ca^{2+} release by the ER ($J_{Release}$), showing how it depends on a $[Ca^{2+}]_i$-sensitive permeability ($\tilde{P}_{ER}$) that is influenced by the activity of RyRs. We then show how these rate descriptions, when taken together with a description of Ca^{2+} extrusion across the plasma membrane, account for several interesting features of Ca^{2+} dynamics described previously, including $[Ca^{2+}]_i$-dependent attenuation of ER Ca^{2+} accumulation during depolarization, caffeine-induced $[Ca^{2+}]_i$ oscillations, and multiple modes of CICR.

Characterization of the ER Ca^{2+} Uptake Pathway

We begin by summarizing evidence that in sympathetic neurons, Ca^{2+} uptake by the ER is controlled by SERCAs. Three observations support this conclusion. First, specific SERCA inhibitors such as thapsigargin (Tg) and t-BuBHQ elicit transient $[Ca^{2+}]_i$ elevations in the absence of extracellular Ca^{2+} (no added Ca^{2+} + 0.2 mM EGTA), indicating that they release Ca^{2+} from an intracellular store (unpublished data), presumably by unmasking ongoing passive Ca^{2+} release that discharges the store. Second, when used at saturating concentra-

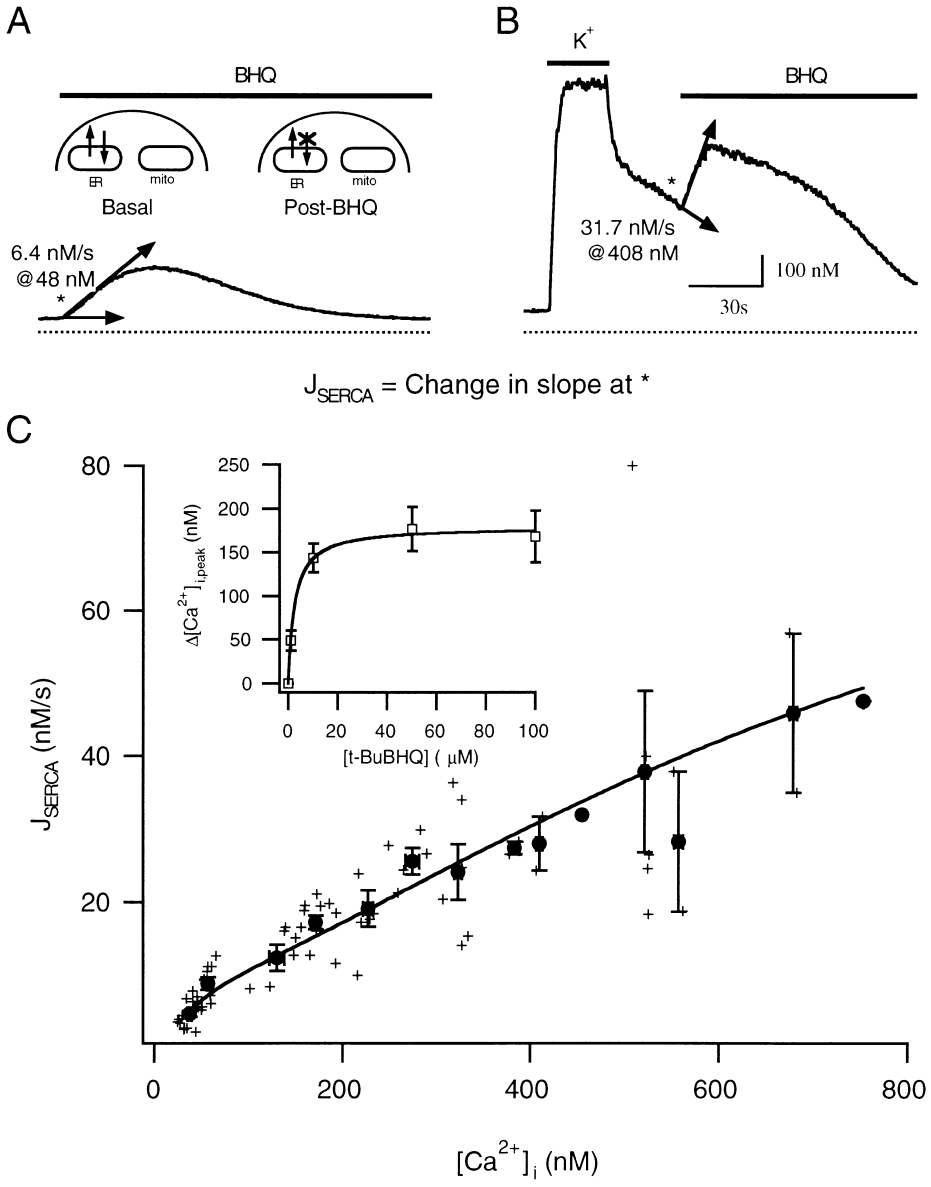

FIGURE 2. Characterization of the ER Ca^{2+} uptake pathway. To measure the rate of Ca^{2+} uptake by the ER (J_{SERCA}), cells were exposed rapidly to 100 μM t-BuBHQ either under resting conditions (A) or when $[Ca^{2+}]_i$ was elevated during the recovery after a 50-mM K^+-induced $[Ca^{2+}]_i$ elevation (B). J_{SERCA} was measured based on the initial change in $d[Ca^{2+}]_i/dt$ after t-BuBHQ application (see diagrams in A). (C) J_{SERCA} increases with $[Ca^{2+}]_i$ at the instant of the perturbation. Data show mean J_{SERCA} over 50-nM intervals ± SEM, representing 76 measurements from six cells. Smooth curve shows an empirical description of the $[Ca^{2+}]_i$ dependence of J_{SERCA} based on Eq. B8, where $V_{max,SERCA}$ = 2,146 nM/s, $EC_{50,SERCA}$ = 30.3 nM, and n_{SERCA} = 2.5. Inset shows the concentration dependence of t-BuBHQ-induced peak $[Ca^{2+}]_i$ elevations, where the smooth curve represents a single site model with maximal response 179 nM and half maximal response at 2.6 μM t-BuBHQ.

tions, pretreatment with one inhibitor occludes responses to the others, arguing that they have a common site of action (unpublished data). Third, pretreatment with a SERCA inhibitor (e.g., Tg) at maximally effective concentrations abolishes responsiveness to other agents that stimulate passive Ca^{2+} release in naive cells by different means (e.g., caffeine; Friel, 1995), indicating that the inhibitors effectively dissipate the gradient favoring Ca^{2+} release, and that SERCAs represent the major, if not the only, pathway for energy-dependent Ca^{2+} uptake by the store. At the concentrations tested, neither of these inhibitors systematically influenced resting $[Ca^{2+}]_i$, indicating that depletion of stores does not elicit capacitative Ca^{2+} entry, in contrast to many nonexcitable cells (Lewis, 1999). Direct measurement of changes in total Ca concentration within the ER and other cellular compartments accompanying Tg- and caffeine-induced $[Ca^{2+}]_i$ transients indicate that the Tg- and caffeine-sensitive store in these cells is the ER (Hongpaisan et al., 2001).

To characterize the rate of ER Ca^{2+} uptake and its regulation by $[Ca^{2+}]_i$, the following protocol was used. Cells were exposed to t-BuBHQ to inhibit Ca^{2+} uptake, and the resulting change in $[Ca^{2+}]_i$ was observed (Fig. 2). The inhibitor was applied rapidly (within ~200 ms) and at a high concentration (100 μM; see Fig. 2 C, inset) to minimize the delay between exposure and cessation of uptake. With this concentration, the delay to the first detectable $[Ca^{2+}]_i$ increase was within one sample interval (200–250 ms), indicating that t-BuBHQ reached its site of action within this time. Moreover, reducing [t-BuBHQ] from 100 to 50 μM, which would be

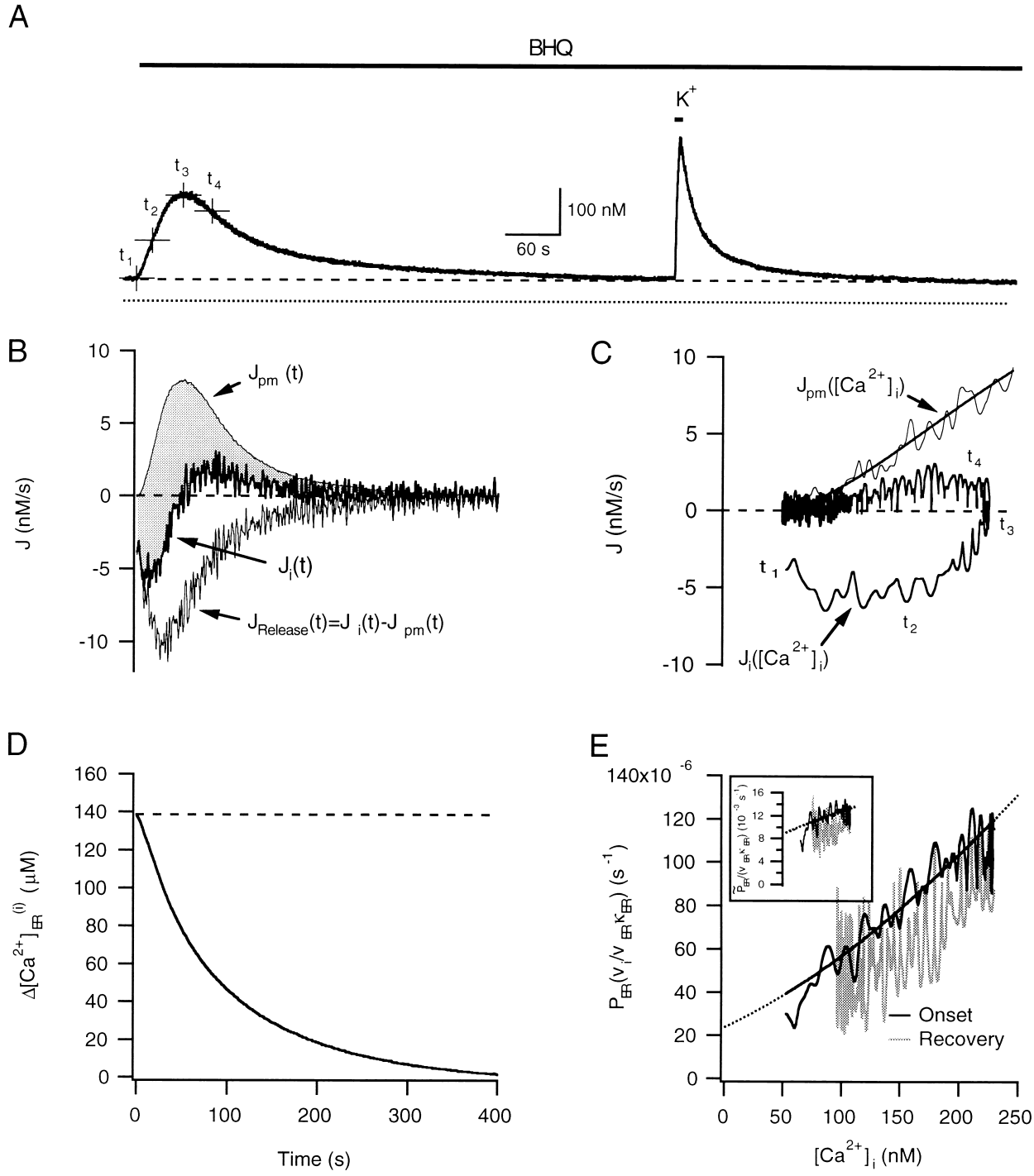

FIGURE 3. Characterization of the ER Ca^{2+} release pathway. (A) Experimental protocol used to characterize the pathway responsible for passive Ca^{2+} release from the ER. During continuous exposure to 1 μM FCCP, cells were exposed rapidly to 100 μM t-BuBHQ, and after $[Ca^{2+}]_i$ returned to its prestimulation level, they were depolarized briefly by exposure to 50 mM K^+ in the continued presence of t-BuBHQ and FCCP. (B) Time course of the Ca^{2+} fluxes underlying the t-BuBHQ-induced $[Ca^{2+}]_i$ transient on the same time scale as in A. J_i is the total cytoplasmic Ca^{2+} flux representing the imbalance between plasma membrane Ca^{2+} extrusion (J_{pm}) and passive Ca^{2+} release from the ER ($J_{Release}$). J_{pm} was calculated based on the recovery after high K^+ depolarization, and $J_{Release}$ was calculated as the difference between J_i and J_{pm} at corresponding times (shaded region). (C) J_{pm} was measured by taking the time derivative of $[Ca^{2+}]_i$ during the recovery after the high K^+-induced $[Ca^{2+}]_i$ elevation in A and plotting against $[Ca^{2+}]_i$. Smooth curve represents a fit to Eq. B6. Also shown is J_i versus $[Ca^{2+}]_i$ during the t-BuBHQ-induced transient. For reference, t_1–t_4 correspond to times indicated in A. J_{pm} was determined at each point in time t during the t-BuBHQ-induced $[Ca^{2+}]_i$ transient by calculating the value of the fitted J_{pm} curve at $[Ca^{2+}](t)$. $J_{Release}$ was determined at each point in time in B as $J_i(t) - J_{pm}([Ca^{2+}]_i(t))$. (D) Plot of $\Delta[Ca^{2+}]^{(i)}_{ER}(t)$, the integral of $J_{Release}\kappa_i$ from the instant of t-BuBHQ addi-

expected to cause the intracellular concentration of the inhibitor to increase more slowly, did not reduce the size of evoked $[Ca^{2+}]_i$ transients (Fig. 2 C, inset), supporting the conclusion that SERCA activity is rapidly inhibited in these experiments.

When t-BuBHQ was applied to resting cells (Fig. 2 A), $[Ca^{2+}]_i$ rose at an initial rate of 6.0 ± 0.6 nM/s; resting $[Ca^{2+}]_i$ in this set of experiments was 43.6 ± 2.2 nM (28 responses in six cells). The initial rate of rise provides a measure of the rate of passive Ca^{2+} release just before the perturbation, and of the rate of Ca^{2+} uptake that balances release under basal conditions (Fig. 2 A, diagrams). The same idea applies under nonsteady-state conditions (e.g., during the recovery after a depolarization-evoked $[Ca^{2+}]_i$ elevation; Fig. 2 B), leading to the generalization that the rate of SERCA-dependent Ca^{2+} uptake is given by the change in slope after rapid SERCA inhibition.

Collected results showing how the rate of Ca^{2+} uptake (J_{SERCA}) varies with $[Ca^{2+}]_i$ are presented in Fig. 2 C. Over the range examined (up to ~800 nM), J_{SERCA} increases monotonically with $[Ca^{2+}]_i$. Although it is difficult to exclude a functional dependence of J_{SERCA} on intraluminal Ca^{2+} concentration, we found that after treatment with ryanodine, which reduces intraluminal total Ca concentration by ~60% (Hongpaisan et al., 2001) and presumably causes a significant reduction in intraluminal free Ca concentration, the resting value of J_{SERCA} was unchanged. This suggests that $[Ca^{2+}]_i$ is the most important variable controlling J_{SERCA} in these experiments, at least under resting conditions. The smooth curve in Fig. 2 C, obtained as described in MATERIALS AND METHODS, provides a description of the composite $[Ca^{2+}]_i$ dependence of J_{SERCA} from basal levels up to ~800 nM.

Characterization of the ER Ca^{2+} Release Pathway

Pathways that may contribute to passive, or energetically downhill, Ca^{2+} release include RyRs, inositol (1,4,5)-trisphosphate receptors ($InsP_3Rs$), as well as an independent leak pathway. To determine the rate of passive Ca^{2+} release via all such pathways ($J_{Release}$) and its dependence on Ca^{2+} concentration, the following experiment was performed (Fig. 3). Cells were exposed to carbonyl cyanide p-(trifluoromethoxy)phenylhydrazone (FCCP), and then were exposed rapidly to 100 μM t-BuBHQ to inhibit SERCA-mediated Ca^{2+} uptake. As before, this elicited a transient $[Ca^{2+}]_i$ rise (Fig. 3 A, left). Since the main, or only, Ca^{2+} fluxes responsible for the t-BuBHQ-induced $[Ca^{2+}]_i$ transient are passive Ca^{2+} release from the ER and Ca^{2+} extrusion across the plasma membrane, measurement of the total Ca^{2+} flux during the transient, along with a characterization of the rate of Ca^{2+} extrusion across the plasma membrane, permits calculation of the rate of passive Ca^{2+} release by subtraction at each point in time during the $[Ca^{2+}]_i$ transient. The rate of Ca^{2+} extrusion was determined from the recovery after a brief, high K^+ depolarization elicited in the continued presence of t-BuBHQ and FCCP (Fig. 3 A, right). Under these conditions, Ca^{2+} extrusion is the primary, or only, mechanism of Ca^{2+} clearance.

Fig. 3 B shows the total cytoplasmic Ca^{2+} flux (J_i) during the t-BuBHQ-induced $[Ca^{2+}]_i$ transient, determined by calculating the derivative of $[Ca^{2+}]_i$ at each point in time (inward fluxes are negative, outward fluxes are positive). J_i was initially negative and increased in magnitude to a peak before declining and changing sign after $[Ca^{2+}]_i$ attained its peak value, to become an outward flux. It then increased to maximum before finally declining to zero.

To determine $J_{Release}$, it was necessary to dissect J_i into its component fluxes. The rate of Ca^{2+} extrusion across the plasma membrane (J_{pm}) was determined by measuring the total Ca^{2+} flux during the recovery after depolarization, and is plotted against $[Ca^{2+}]_i$ in Fig. 3 C; for comparison, J_i is also plotted throughout the t-BuBHQ-induced transient. In a previous study, it was shown that at each point in time, J_{pm} depends on the $[Ca^{2+}]_i$ level at that time (Colegrove et al., 2000a). This made it possible to determine the rate of Ca^{2+} extrusion at each time point during the t-BuBHQ-induced transient based on the magnitude of J_{pm} during the recovery after repolarization at the corresponding $[Ca^{2+}]_i$ level. The time course of J_{pm} determined in this way is shown in Fig. 3 B and parallels the $[Ca^{2+}]_i$ response. Subtracting J_{pm} from J_i at each point in time then gives the remaining Ca^{2+} flux (Fig. 3 B, shaded region). Since these measurements were performed in the presence of FCCP and a saturating concentration of t-BuBHQ, the remaining flux ($J_{Release}$) is expected to represent the rate of passive Ca^{2+} release from the ER (Fig. 3 B). If cytoplasmic and intraluminal buffers equilibrate rapidly with Ca^{2+} and the latter bind Ca^{2+} with low affinity, then at each instant in time, the prod-

tion, minus the integral over the entire transient. Plot is on the same time scale as A and B. (E) $[Ca^{2+}]_i$ dependence of $P_{ER}(v_i/v_{ER}\kappa_{ER})$ during the t-BuBHQ-induced $[Ca^{2+}]_i$ transient. Dark and light traces represent the onset and recovery, respectively. $P_{ER}(v_i/v_{ER}\kappa_{ER})$ was calculated from the ratio of $J_{Release}(t)$ to $\Delta[Ca^{2+}]^{(i)}_{ER}(t)$ as described in APPENDIX A. Smooth curve represents Eqs. B10 and B11, where $\tilde{P}_{basal}$ = 0.009 s^{-1}, $\tilde{P}_{max,RYR}$ = 0.05 s^{-1}, $EC_{50,RyR}$ = 2,641 nM, n_{RyR} = 0.96, and κ_i is described by the smooth curve in Fig. 1 D. Inset gives $\tilde{P}_{ER}/(v_{ER}\kappa_{ER})$, obtained after scaling $P_{ER}(v_i/v_{ER}\kappa_{ER})$ by κ_i. Smooth curve represents Eq. B10 using identical parameter values. At low $[Ca^{2+}]_i$ during the recovery, $P_{ER}(v_i/v_{ER}\kappa_{ER})$ is the ratio of two small and noisy numbers, contributing to the scatter of these measurements; for clarity, noisy values during the recovery below 100 nM are not shown.

uct $J_{Release}\kappa_i$ should be directly proportional to the net ER Ca^{2+} flux, and, therefore, to the rate at which $[Ca^{2+}]_{ER}$ changes with time (see APPENDIX A). The properties of $J_{Release}$ are revealing. During the entire t-BuBHQ-induced $[Ca^{2+}]_i$ transient, $J_{Release}$ is negative, which is indicative of Ca^{2+} release. During the rising phase, the magnitude of $J_{Release}$ increases to a peak. This increase occurs even though the driving force for passive Ca^{2+} release should be falling ($[Ca^{2+}]_i$ is rising and the intraluminal Ca^{2+} concentration is falling). As discussed in connection with Fig. 2, with our application protocol, t-BuBHQ appears to block SERCAs rapidly (within 200 ms) and completely, arguing that the initial increase in $J_{Release}$ observed in control cells does not simply reflect the time required for the inhibitor to act. This is supported by the finding that, in ryanodine-treated cells, the magnitude of $J_{Release}$ declines monotonically after t-BuBHQ application (see Fig. 4). This suggests that the pathway responsible for passive Ca^{2+} release includes a $[Ca^{2+}]_i$-sensitive permeability.

Given measurements of $J_{Release}$, along with a description of the intraluminal Ca^{2+} concentration, it is possible to characterize the Ca^{2+} permeability of the ER and test the idea that it is sensitive to $[Ca^{2+}]$. When ER Ca^{2+} uptake is inhibited, $J_{Release}$ gives the net ER Ca^{2+} flux referred to the effective cytoplasmic volume, so multiplying by the ratio of effective cytoplasmic and intraluminal volumes ($v_i\kappa_i/v_{ER}\kappa_{ER}$) gives the rate at which $[Ca^{2+}]_{ER}$ changes with time. Integration of this quantity from the instant of t-BuBHQ application to the time t thus provides a measure of the change in $[Ca^{2+}]_{ER}$ relative to its initial value just before the perturbation. Subtracting the integral during the entire t-BuBHQ-induced $[Ca^{2+}]_i$ transient gives the change in concentration relative to its final basal value. As shown in APPENDIX A, this latter quantity, which we call $\Delta[Ca^{2+}]_{ER}(t)$, is given by Eq. 2:

$$\begin{aligned}\Delta[Ca^{2+}]_{ER}(t) &= -\frac{v_i}{v_{ER}\kappa_{ER}}\int_t^{\infty} J_{Release}\kappa_i dt' \\ &= \frac{v_i}{v_{ER}\kappa_{ER}}\Delta[Ca^{2+}]_{ER}^{(i)}(t),\end{aligned} \tag{2}$$

where minus the integral ($\Delta[Ca^{2+}]_{ER}^{(i)}$) can be interpreted as the change in total cytoplasmic Ca concentration that would occur if from time t onward, $J_{Release}$ were deposited into a closed compartment having the same volume as the cytoplasm. Accordingly, the initial value ($\Delta[Ca^{2+}]_{ER}^{(i)}(0)$) provides information about the resting Ca^{2+} concentration within the ER. The relationship is (Eq. 3):

$$[Ca^{2+}]_{ER}(0) = [Ca^{2+}]_{ER}(\infty) + \frac{v_i}{v_{ER}\kappa_{ER}}\Delta[Ca^{2+}]_{ER}^{(i)}(0). \tag{3}$$

A similar approach to assessing changes in ER Ca^{2+} concentration in T cells was described previously by Bergling et al. (1998).

Before using $J_{Release}$ and $\Delta[Ca^{2+}]_{ER}^{(i)}(t)$ to characterize the Ca^{2+} permeability of the ER, it is important to determine if these quantities have the expected properties. During the entire t-BuBHQ-induced $[Ca^{2+}]_i$ transient, the sign of $J_{Release}$ is indicative of net Ca^{2+} release, and correspondingly $\Delta[Ca^{2+}]_{ER}^{(i)}(t)$ declines monotonically from the point of t-BuBHQ addition (Fig. 3 D). Analysis of sympathetic neurons gives an estimate of 10–20 for v_i/v_{ER} (unpublished data); although measurements of κ_{ER} have not been made in these cells, values have been reported in other cells: ~17 in AtT-20 cells (Wu et al., 2001) and ~20 in pancreatic acinar cells (Mogami et al., 1999). Based on these values, $v_i/(v_{ER}\kappa_{ER})$ can be estimated to be ~0.5–1.2. Thus, the ~140-μM decline in $\Delta[Ca^{2+}]_{ER}^{(i)}$ shown in Fig. 3 C would correspond to a 70–168-μM decline in $[Ca^{2+}]_{ER}$. Since the basal value of $[Ca^{2+}]_{ER}$ after treatment with t-BuBHQ ($[Ca^{2+}]_{ER}(\infty)$) would be expected to approximate the resting cytoplasmic Ca^{2+} concentration (~50–100 nM), using Eq. 3 we arrive at an estimated initial value of $[Ca^{2+}]_{ER}$ ~70.1–168.1 μM. This is consistent with the value obtained from the reduction in total ER Ca concentration induced by Tg, as determined from electron probe microanalysis in these cells (~2 mM; Hongpaisan et al., 2001) using the same values for κ_{ER}: $\Delta[Ca^{2+}]_{ER} \sim 2\ mM/20 = 100\ \mu M$. It should be noted that because slow net Ca^{2+} release is increasingly difficult to resolve as $[Ca^{2+}]_i$ approaches its resting level, it is difficult to determine when $J_{Release}$ is truly zero and Ca^{2+} within the ER is in equilibrium with the cytoplasmic compartment. Therefore, it is possible that the initial value of $\Delta[Ca^{2+}]_{ER}^{(i)}$, and hence our estimations of basal $[Ca^{2+}]_{ER}$, underestimate the actual values.

Measurements of $J_{Release}$ and $\Delta[Ca^{2+}]_{ER}^{(i)}(t)$, along with the characterization of κ_i from Fig. 1, can now be used to provide information about the Ca^{2+} permeability of the ER ($\tilde{P}_{ER}$). $\tilde{P}_{ER}$ is defined operationally by Eq. 4:

$$\begin{aligned}J_{Release} &= \frac{\tilde{J}_{Release}}{v_i\kappa_i} \\ &= \frac{\tilde{P}_{ER}([Ca^{2+}]_i - [Ca^{2+}]_{ER})}{v_i\kappa_i} \\ &\equiv P_{ER}([Ca^{2+}]_i - [Ca^{2+}]_{ER}),\end{aligned} \tag{4}$$

where P_{ER} is a lumped parameter giving the ratio of $\tilde{P}_{ER}$ to $v_i\kappa_i$, and $[Ca^{2+}]_{ER}(t)$ is the free Ca concentration within the ER at time t. $\tilde{P}_{ER}$ would be expected to depend on the number, open probability, and unitary Ca^{2+} permeability of ryanodine-sensitive Ca^{2+} release channels expressed in these cells, as well as other channels that are permeable to Ca^{2+} and influence the rate of passive Ca^{2+} release. In particular, the $[Ca^{2+}]_i$ depen-

dence of $\tilde{P}_{ER}$ should provide information about how the activity of these channels varies with $[Ca^{2+}]_i$. In general, $\tilde{P}_{ER}$ could be influenced by $[Ca^{2+}]_i$, $[Ca^{2+}]_{ER}$, and could show explicit time dependence (e.g., as a result of desensitization). Finally, P_{ER} would be expected to show a composite $[Ca^{2+}]_i$ dependence representing properties of both $\tilde{P}_{ER}$ and κ_i.

Given measurements of $J_{Release}$ and $([Ca^{2+}]_i - [Ca^{2+}]_{ER})$, P_{ER} could be determined from the ratio $J_{Release}/([Ca^{2+}]_i - [Ca^{2+}]_{ER})$ at each point in time during the t-BuBHQ-induced $[Ca^{2+}]_i$ transient; measurements of κ_i would then make possible to obtain information about $\tilde{P}_{ER}$. This approach requires information about $[Ca^{2+}]_{ER}(t)$. Although single cell measurements of $[Ca^{2+}]_{ER}(t)$ are not available, it is shown in APPENDIX A that $([Ca^{2+}]_i - [Ca^{2+}]_{ER})$ can be approximated by $-(v_i/v_{ER}\kappa_{ER})\Delta[Ca^{2+}]^{(i)}_{ER}$, making it possible to rewrite Eq. 4 as Eq. 5:

$$J_{Release}(t) \approx -\frac{P_{ER}(t)v_i}{v_{ER}\kappa_{ER}}\Delta[Ca^{2+}]^{(i)}_{ER}(t), \quad (5)$$

and to obtain a quantity that is proportional to P_{ER} from measured values,

$$P_{ER}(t)\left[\frac{v_i}{v_{ER}\kappa_{ER}}\right] \approx -\frac{J_{Release}(t)}{\Delta[Ca^{2+}]^{(i)}_{ER}(t)}, \quad (6)$$

which is valid as long as $[Ca^{2+}]_{ER}$ is much larger than $[Ca^{2+}]_i$ (see APPENDIX A). Fig. 3 E shows $P_{ER}(v_i/v_{ER}\kappa_{ER})$ plotted against $[Ca^{2+}]_i$ during the t-BuBHQ-induced $[Ca^{2+}]_i$ transient, calculated according to Eq. 6. The dark noisy trace shows $P_{ER}(v_i/v_{ER}\kappa_{ER})$ during the rising phase of the transient, and the light trace represents the recovery phase. Three features of these measurements should be noted. First, $P_{ER}(v_i/v_{ER}\kappa_{ER})$ is not constant, but increases monotonically with $[Ca^{2+}]_i$ over the range ~50–250 nM. Second, the $[Ca^{2+}]_i$ dependence of $P_{ER}(v_i/v_{ER}\kappa_{ER})$ during the onset and recovery (dark and light traces, respectively) is very similar. In other words, for a given value of $[Ca^{2+}]_i$, $P_{ER}(v_i/v_{ER}\kappa_{ER})$ has essentially the same magnitude during both the onset and the recovery. Since the intraluminal Ca^{2+} concentration is expected to be very different during these phases of the t-BuBHQ-induced $[Ca^{2+}]_i$ transient, it appears that $P_{ER}(v_i/v_{ER}\kappa_{ER})$ depends much more strongly on $[Ca^{2+}]_i$ than on $[Ca^{2+}]_{ER}$. Moreover, if the underlying permeability undergoes desensitization, it must be very rapid, or very weak, compared with the $[Ca^{2+}]_i$-dependent changes observed in these experiments. Finally, extrapolation of $P_{ER}(v_i/v_{ER}\kappa_{ER})$ to $[Ca^{2+}]_i = 0$ gives an estimate of the basal Ca^{2+} permeability of the ER (Fig. 3 E, dotted trace); however, since this value is based on extrapolation, there is uncertainty about its precise value. Importantly, these properties are shared by the macroscopic Ca^{2+} permeability. Fig. 3 E (inset) shows $\tilde{P}_{ER}/v_{ER}\kappa_{ER}$, obtained after scaling $P_{ER}(v_i/v_{ER}\kappa_{ER})$ by κ_i, indicating that the macroscopic Ca^{2+} permeability of the ER depends on $[Ca^{2+}]_i$. Results presented in the next section provide evidence that this $[Ca^{2+}]_i$-dependent permeability is dominated by ryanodine receptors.

Changes in ER Ca^{2+} Permeability Induced by Caffeine and Ryanodine

A number of observations indicate that sympathetic neurons express functional RyRs (Kuba and Nishi, 1976; Lipscombe et al., 1988; Friel and Tsien, 1992a,b; Hua et al., 1993; Akita and Kuba, 2000) that would contribute to the macroscopic Ca^{2+} permeability of the ER, so we performed experiments to determine if $\tilde{P}_{ER}$ is sensitive to pharmacological modifiers of RyRs (Zucchi and Roncha-Testoni, 1997). Fig. 4 shows t-BuBHQ-induced $[Ca^{2+}]_i$ transients (Fig. 4 A) and the corresponding measurements of $J_{Release}$ (Fig. 4 B) and $\Delta[Ca^{2+}]^{(i)}_{ER}$ (Fig. 4 C) under control conditions, during continuous exposure to caffeine (after the caffeine-induced $[Ca^{2+}]_i$ transient) and after treatment with ryanodine, which rendered cells unresponsive to caffeine. Fig. 4 D compares the $[Ca^{2+}]_i$ dependence of $P_{ER}(v_i/v_{ER}\kappa_{ER})$ for each cell whose responses are illustrated in Fig. 4, A–C; population results are shown in Fig. 4 E. In the presence of caffeine, t-BuBHQ-induced $[Ca^{2+}]_i$ transients are faster, and $\Delta[Ca^{2+}]^{(i)}_{ER}$ declines more rapidly, compared with controls, reflecting an approximately threefold increase in the peak magnitude of $J_{Release}$. In contrast, after treatment with ryanodine, the evoked $[Ca^{2+}]_i$ transients are slower, and $\Delta[Ca^{2+}]^{(i)}_{ER}$ declines more slowly than the control, reflecting a steady decline in $J_{Release}$ that contrasts markedly with the initial increase seen both in the control case and in the presence of caffeine. Given that the magnitude of $J_{Release}$ declines monotonically from the instant of t-BuBHQ application in ryanodine-treated cells, it is unlikely that the initial increase in $J_{Release}$ observed in control and caffeine-treated cells occurs simply because the inhibitor acts slowly, or because of $[Ca^{2+}]_i$-dependent changes in cytoplasmic Ca^{2+} buffering strength. It also was found that the initial value of $\Delta[Ca^{2+}]^{(i)}_{ER}$ followed the order: control (115 ± 12 μM, four cells) is greater than +caffeine (38 ± 4 μM, four cells) is greater than +ryanodine (20 ± 3 μM, three cells). Neither caffeine nor ryanodine had a systematic effect on J_{pm} (unpublished data). These actions of caffeine and ryanodine on t-BuBHQ-induced $[Ca^{2+}]_i$ transients are consistent with their effects on $P_{ER}(v_i/v_{ER}\kappa_{ER})$ and $\tilde{P}_{ER}/(v_{ER}\kappa_{ER})$ (Fig. 4 D). In the presence of caffeine and ryanodine, $\tilde{P}_{ER}/(v_{ER}\kappa_{ER})$ shows higher values at resting $[Ca^{2+}]_i$ than the control, accounting for the lower basal values of $\Delta[Ca^{2+}]^{(i)}_{ER}$ (Fig. 4 C). In the presence of caffeine, $\tilde{P}_{ER}/(v_{ER}\kappa_{ER})$ also increases more steeply with $[Ca^{2+}]_i$ than in the control and shows a supralinear $[Ca^{2+}]_i$ dependence, which presumably contributes to the accel-

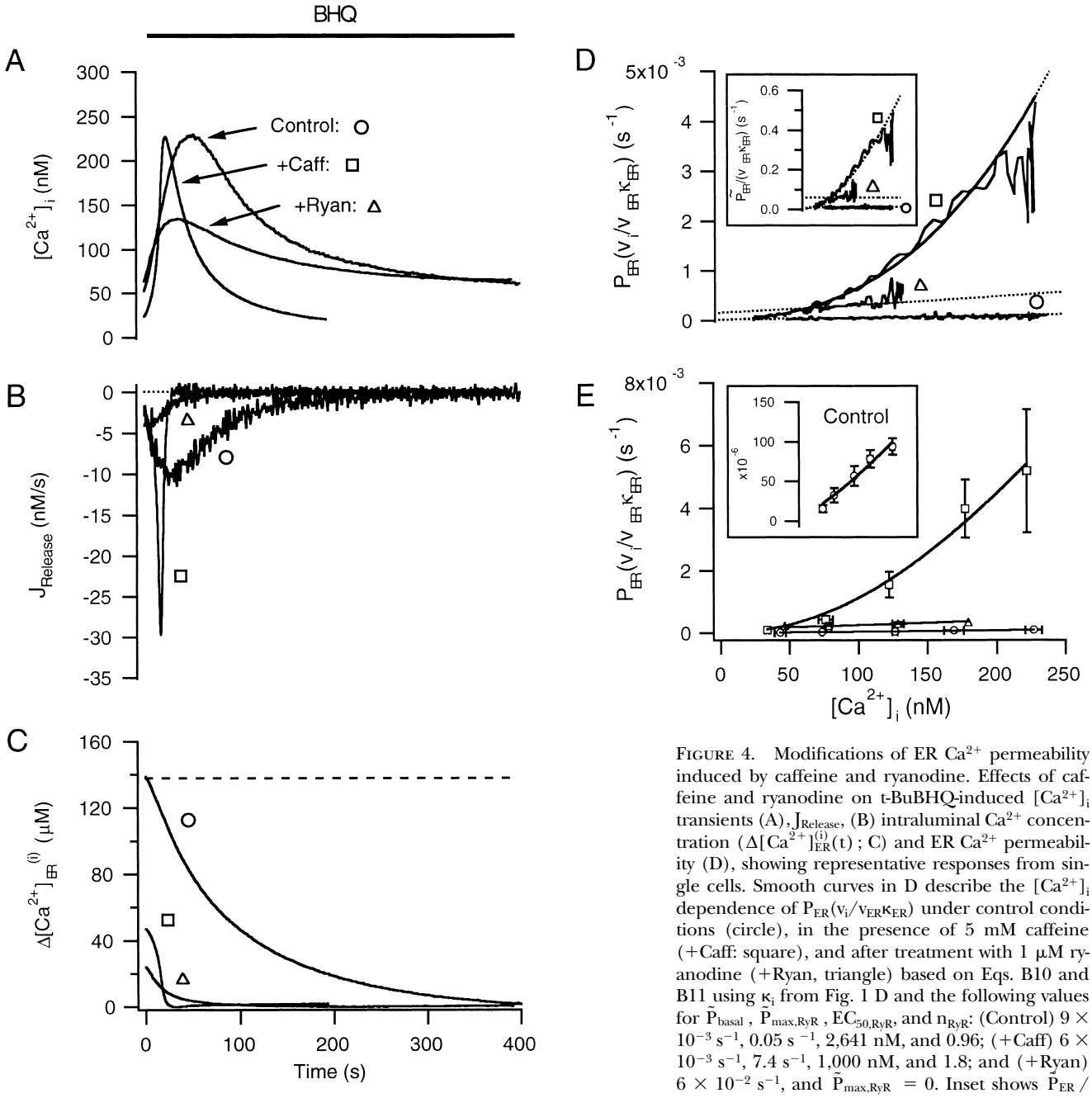

FIGURE 4. Modifications of ER Ca^{2+} permeability induced by caffeine and ryanodine. Effects of caffeine and ryanodine on t-BuBHQ-induced $[Ca^{2+}]_i$ transients (A), $J_{Release}$, (B) intraluminal Ca^{2+} concentration ($\Delta[Ca^{2+}]_{ER}^{(i)}(t)$; C) and ER Ca^{2+} permeability (D), showing representative responses from single cells. Smooth curves in D describe the $[Ca^{2+}]_i$ dependence of $P_{ER}(v_i/v_{ER}\kappa_{ER})$ under control conditions (circle), in the presence of 5 mM caffeine (+Caff: square), and after treatment with 1 μM ryanodine (+Ryan, triangle) based on Eqs. B10 and B11 using κ_i from Fig. 1 D and the following values for $\tilde{P}_{basal}$, $\tilde{P}_{max,RyR}$, $EC_{50,RyR}$, and n_{RyR}: (Control) 9×10^{-3} s^{-1}, 0.05 s^{-1}, 2,641 nM, and 0.96; (+Caff) 6×10^{-3} s^{-1}, 7.4 s^{-1}, 1,000 nM, and 1.8; and (+Ryan) 6×10^{-2} s^{-1}, and $\tilde{P}_{max,RyR} = 0$. Inset shows $\tilde{P}_{ER}/(v_{ER}\kappa_{ER})$ obtained after multiplying $P_{ER}(v_i/v_{ER}\kappa_{ER})$ by κ_i. Cells were exposed to 1 μM FCCP throughout the recording. Control cell is from Fig. 3 (note different ordinate scale in D). (E) Collected measurements of $P_{ER}(v_i/v_{ER}\kappa_{ER})$ under control conditions (four cells), in the presence of 5 mM caffeine (four cells), and after treatment with 1 μM ryanodine (three cells). Smooth curves represent fits based on Eqs. B10 and B11. Measurements were averaged over 50-nM $[Ca^{2+}]_i$ intervals, and the mean ± SEM were determined for each interval from multiple cells studied under the same condition. Inset shows collected control measurements on an expanded ordinate scale.

erated $[Ca^{2+}]_i$ rise (Fig. 4, A and B). After ryanodine treatment, the $[Ca^{2+}]_i$ dependence of $P_{ER}(v_i/v_{ER}\kappa_{ER})$ could be accounted for simply by the $[Ca^{2+}]_i$ dependence of κ_i, indicating that, under these conditions, $\tilde{P}_{ER}/(v_{ER}\kappa_{ER})$ does not vary with $[Ca^{2+}]_i$, accounting for the monotonic decline in the magnitude of $J_{Release}$ (Fig. 4 B) and the slower $[Ca^{2+}]_i$ transient (Fig. 4 A). Each effect is consistent with known properties of RyRs and their modification by caffeine and ryanodine (Rousseau et al., 1987, 1988). Overall, the results illustrate how a caffeine- and ryanodine-sensitive Ca^{2+} permeability representing the activity of a population of RyRs contributes to passive Ca^{2+} release from the ER. Importantly, the properties of $\tilde{P}_{ER}$ in ryanodine-treated cells sug-

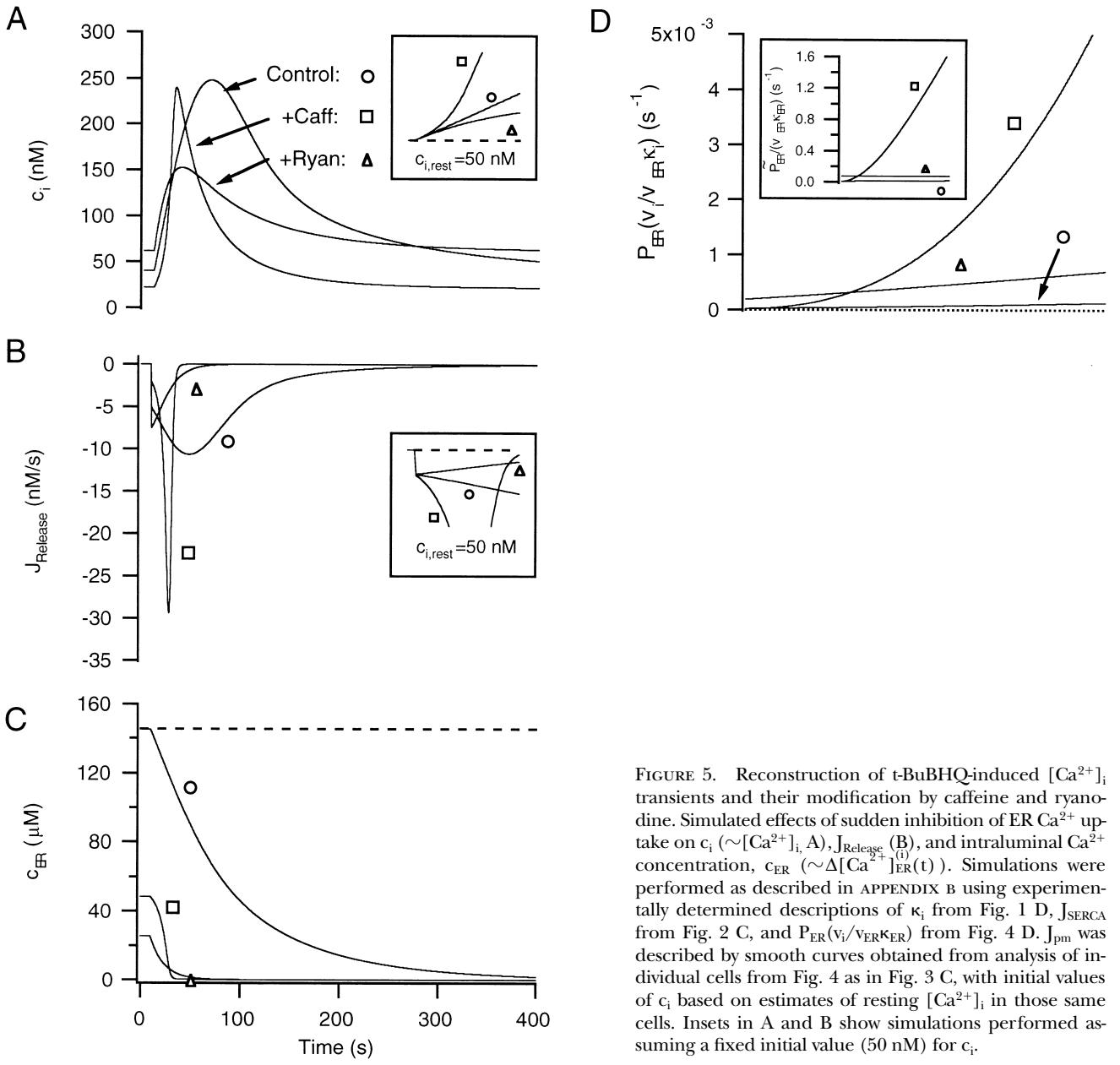

FIGURE 5. Reconstruction of t-BuBHQ-induced $[Ca^{2+}]_i$ transients and their modification by caffeine and ryanodine. Simulated effects of sudden inhibition of ER Ca^{2+} uptake on c_i ($\sim[Ca^{2+}]_i$, A), $J_{Release}$ (B), and intraluminal Ca^{2+} concentration, c_{ER} ($\sim\Delta[Ca^{2+}]^{(i)}_{ER}(t)$). Simulations were performed as described in APPENDIX B using experimentally determined descriptions of κ_i from Fig. 1 D, J_{SERCA} from Fig. 2 C, and $P_{ER}(v_i/v_{ER}\kappa_{ER})$ from Fig. 4 D. J_{pm} was described by smooth curves obtained from analysis of individual cells from Fig. 4 as in Fig. 3 C, with initial values of c_i based on estimates of resting $[Ca^{2+}]_i$ in those same cells. Insets in A and B show simulations performed assuming a fixed initial value (50 nM) for c_i.

gests that RyRs are responsible for most of the $[Ca^{2+}]_i$ dependence of ER Ca^{2+} permeability when $[Ca^{2+}]_i <$ 250 nM and InsP3-generating agonists are not present.

Reconstruction of t-BuBHQ-induced Ca^{2+} Responses and the Underlying Ca^{2+} Fluxes

To determine if the rate descriptions presented above are sufficient to account for the dynamics of cytoplasmic and intraluminal Ca^{2+} concentration during t-BuBHQ-induced $[Ca^{2+}]_i$ transients, simulations were performed using the experimentally determined descriptions of J_{SERCA}, J_{pm}, $P_{ER}(v_i/v_{ER}\kappa_{ER})$, and κ_i, approximating $v_i/v_{ER}\kappa_{ER}$ by unity. In displaying the results, simulated Ca^{2+} concentrations are designated by c_i and c_{ER} to distinguish them from measured quantities. To facilitate comparison with responses from cells in Fig. 4, simulations were performed using the transport descriptions and initial $[Ca^{2+}]_i$ values obtained from those same cells. It was found that the simulations reproduce the experimental observations quite well, including the relative values of basal c_{ER} and the time courses of c_i, $J_{Release}$, and c_{ER} (Fig. 5). This leads to three conclusions. First, J_{pm}, J_{SERCA}, and $\tilde{P}_{ER}$ describe the main Ca^{2+} transport pathways responsible for cytoplasmic and intraluminal Ca^{2+} dynamics after rapid SERCA inhibition. Second, the equations used to describe these pathways do not ignore variables that are important for the dynamics of $[Ca^{2+}]_i$ and $\Delta[Ca^{2+}]^{(i)}_{ER}$. Third,

the functional dependence of the fluxes on $[Ca^{2+}]_i$ and $[Ca^{2+}]_{ER}$ is sufficiently accurate to reproduce the salient features of the time courses of $[Ca^{2+}]_i$ and $\Delta[Ca^{2+}]_{ER}^{(i)}$. Thus, when mitochondrial Ca^{2+} transport is suppressed, the initial distribution of intracellular Ca^{2+}, as well as the dynamics of Ca^{2+} after inhibition of SERCAs, can be explained in terms of the properties of J_{pm}, J_{SERCA}, $\tilde{P}_{ER}$, and κ_i.

The Properties of J_{pm}, J_{SERCA}, $P_{ER}(v_i/v_{ER}\kappa_{ER})$, and κ_i Account for Ca^{2+} Dynamics during Depolarization-evoked Ca^{2+} Entry

We have shown that when $[Ca^{2+}]_i$ is low (less than or equal to ~350 nM) during weak depolarization, the ER normally accumulates Ca^{2+}, and that after treatment with ryanodine, the same stimuli lead to enhanced ER Ca^{2+} accumulation (Albrecht et al., 2001). We asked if the properties of J_{pm}, J_{SERCA} $P_{ER}(v_i/v_{ER}\kappa_{ER})$ and κ_i described above account for these observations. Fig. 6 shows simulations of depolarization-induced changes in $[Ca^{2+}]_i$ and $[Ca^{2+}]_{ER}$ using a measured Ca^{2+} current (I_{Ca}) as the basis for calculating the rate of stimulated Ca^{2+} entry (Fig. 6 A). Mitochondrial Ca^{2+} uptake was taken into consideration as described in Colegrove et al. (2000b) to facilitate comparison with measurements performed under voltage clamp in the absence of FCCP (Albrecht et al., 2001). Using parameters for $P_{ER}(v_i/v_{ER}\kappa_{ER})$ obtained under control conditions, Ca^{2+} entry produces a c_i elevation that is accompanied by weak ER Ca^{2+} accumulation; consequently, the $[Ca^{2+}]_i$ response is slightly accelerated when uptake is inhibited with Tg, as observed experimentally (Albrecht et al., 2001). Using $P_{ER}(v_i/v_{ER}\kappa_{ER})$ parameters taken from ryanodine-treated cells, Ca^{2+} entry elicits a slower rise in c_i but a more robust increase in c_{ER}, also as observed experimentally (Albrecht et al., 2001). Finally, using $P_{ER}(v_i/v_{ER}\kappa_{ER})$ parameters from caffeine-treated cells, $[Ca^{2+}]_i$ rises more rapidly in response to the same stimulus in concert with net Ca^{2+} release. Net Ca^{2+} release occurs in this case because $J_{Release}$ increases more steeply with c_i than does J_{SERCA} over this c_i range. Resting c_{ER} is lower in this and the +Ryan case because basal $P_{ER}(v_i/v_{ER}\kappa_{ER})$ is higher than it is under control conditions. These results validate the quantitative model presented in our previous study (Albrecht et al., 2001).

Comparing ER Ca^{2+} uptake and release rates shows how activation of the CICR pathway influences net ER Ca^{2+} transport and c_i and c_{ER} dynamics during such weak stimuli (Fig. 7). Before stimulation, ER Ca^{2+} uptake and release rates are in balance, accounting for the steady resting value of c_{ER}. The resting rate of release is not modified by ryanodine because while $\tilde{P}_{ER}$ is increased, the driving force is reduced, such that their product is unchanged. Under control conditions (Fig. 7 B), stimulation leads to Ca^{2+} accumulation by the ER (Fig. 7 B, dark trace) because J_{SERCA} increases more rap-

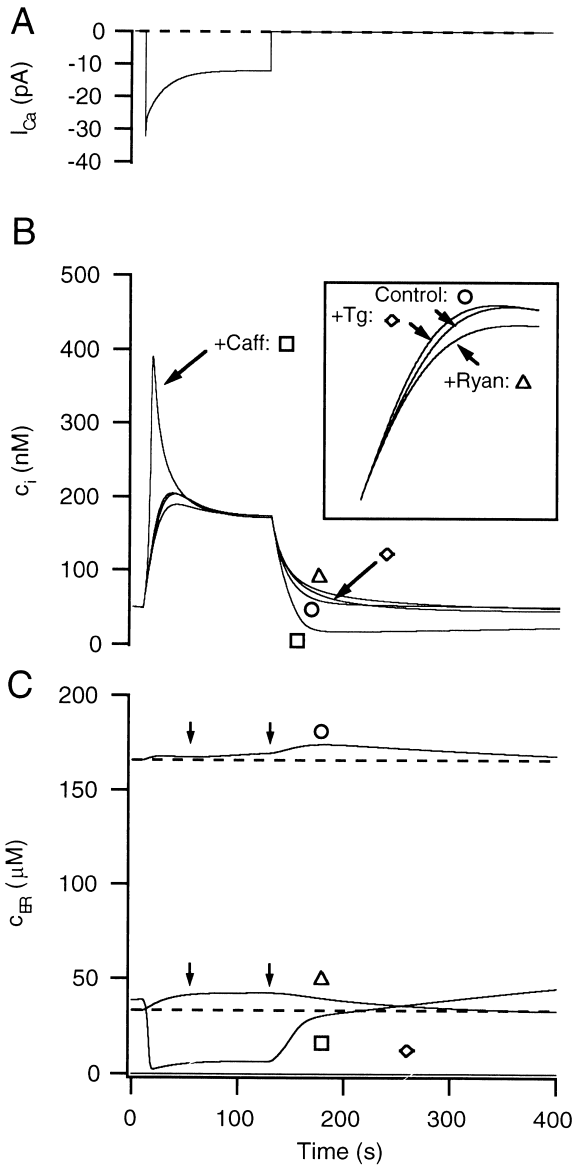

FIGURE 6. Simulated responses to depolarization-evoked Ca^{2+} entry and their sensitivity to modifications of ER Ca^{2+} transport. Simulated changes in c_i (B) and c_{ER} (C) resulting from stimulated Ca^{2+} entry (A). For each simulation, J_{SERCA} was described as in Fig. 2 C, except for the case (+Tg) where $V_{max,SERCA} = 0$, and J_{pm} was described by the smooth curve from the control cell in Fig. 3 C. $P_{ER}(v_i/v_{ER}\kappa_{ER})$ was represented by the smooth curves in Fig. 4 D. In the case of +Tg, $P_{ER}(v_i/v_{ER}\kappa_{ER})$ was described as in the control cell. I_{Ca} is based on a measured Ca^{2+} current elicited by a 40-s depolarization to −35 mV, scaled in amplitude, and extrapolated in time, with tail current omitted. $c_o = 2$ mM and $v_{ER}\kappa_{ER}/v_i = 1$. Mitochondrial Ca^{2+} uptake was described as in Colegrove et al. (2000b) without release to facilitate comparison with experiments performed under voltage clamp in cells with low intracellular Na^+, which inhibits release. Arrows in C indicate the 45- and 120-s time points at which measurements of total ER Ca concentration are available during steady depolarization in the absence and presence of ryanodine (Albrecht et al., 2001).

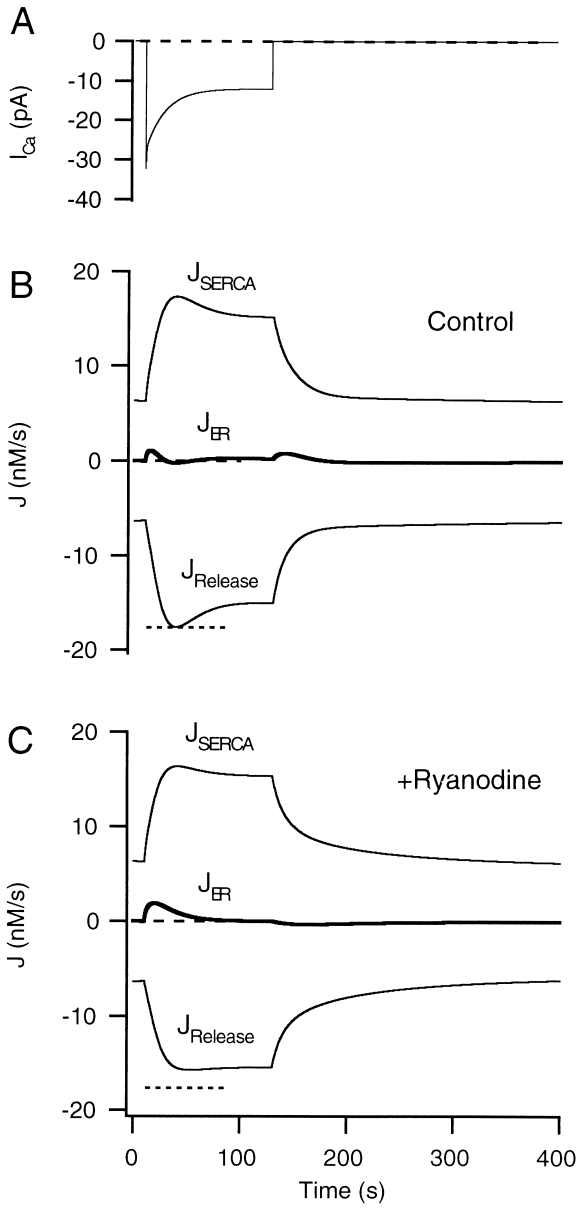

FIGURE 7. Effects of CICR activation on the interplay between ER Ca^{2+} uptake and release rates. Simulated changes in the rate of net ER Ca^{2+} transport (J_{ER}, dark trace) and its components J_{SERCA} and $J_{Release}$ (light traces) during and after stimulated Ca^{2+} entry under control conditions (B) and after inhibiting CICR by setting $\tilde{P}_{max,RyR} = 0$ (C). In each case, the ER accumulates Ca^{2+} during stimulation, but in the control case, the rate of Ca^{2+} accumulation is reduced by activation of the c_i-sensitive permeability. Dashed horizontal lines in B and C mark the maximal rate of Ca^{2+} release during stimulation under control conditions. All parameters are the same as in Fig. 6 (Control, +Ryan).

idly than $J_{Release}$. J_{SERCA} increases because of its intrinsic c_i dependence, whereas $J_{Release}$ rises in magnitude because of two factors: an increase in driving force (since c_{ER} rises more rapidly than c_i) and an increase in $\tilde{P}_{ER}$. The c_i-dependent increase in $\tilde{P}_{ER}$ accelerates the increase in $J_{Release}$, reducing the imbalance between J_{SERCA} and $J_{Release}$, ultimately causing the ER to be a less powerful Ca^{2+} buffer. After inhibiting the c_i-dependent activation of $\tilde{P}_{ER}$ (Fig. 7 C), the magnitude of $J_{Release}$ increases more slowly in response to an increase in driving force only, and this exaggerates the imbalance between J_{SERCA} and $J_{Release}$, leading to enhanced Ca^{2+} accumulation. As a result, the ER becomes a stronger buffer, as observed experimentally (Albrecht et al., 2001).

Properties of $P_{ER}(v_i/v_{ER}\kappa_{ER})$ Account for Caffeine-induced $[Ca^{2+}]_i$ Oscillations

Previous work has shown that when caffeine-treated sympathetic neurons are depolarized to stimulate Ca^{2+} entry, $[Ca^{2+}]_i$ rises rapidly to produce a spike and then, in many cases, oscillates (Lipscombe et al., 1988; Nohmi et al., 1992; Friel and Tsien, 1992b). To determine if these $[Ca^{2+}]_i$ oscillations can be accounted for by the interplay between J_{pm}, J_{SERCA}, and $P_{ER}(v_i/v_{ER}\kappa_{ER})$, simulations were performed using descriptions of J_{pm} and J_{SERCA} from control cells and of $P_{ER}(v_i/v_{ER}\kappa_{ER})$ from caffeine-treated cells. Although Ca^{2+} entry led to a steady increase in c_i when Ca^{2+} uptake by the store was inhibited (Fig. 8, +Tg, dotted traces), oscillations were observed when both uptake and release pathways were enabled. The oscillations were much like those observed experimentally when caffeine-treated sympathetic neurons are depolarized by exposure to high K^+ (Friel and Tsien, 1992b). Using descriptions of $P_{ER}(v_i/v_{ER}\kappa_{ER})$ from control and caffeine-treated cells contributing to the collected results in Fig. 4 E indicates that depolarization-evoked Ca^{2+} entry does not elicit c_i oscillations when control $P_{ER}(v_i/v_{ER}\kappa_{ER})$ descriptions are used (4/4 cells), whereas oscillations can be elicited when descriptions are taken from caffeine-treated cells (4/4 cells). Thus, the quantitative descriptions of ER Ca^{2+} uptake and release pathways obtained using t-BuBHQ-induced perturbations account for the observation that membrane depolarization typically elicits $[Ca^{2+}]_i$ oscillations in caffeine-treated cells, but not in untreated cells.

Quantitative Basis for Multiple Modes of CICR in Sympathetic Neurons

Measurements in sympathetic neurons implicate distinct modes of CICR that operate over different ranges of $[Ca^{2+}]_i$ (Albrecht et al., 2001, Hongpaisan et al., 2001). When $[Ca^{2+}]_i$ is low, the ER accumulates Ca^{2+} at a rate that is reduced by activation of the CICR pathway (Mode 1 CICR). At higher $[Ca^{2+}]_i$ levels, the ER releases Ca^{2+}, either at a rate that is slower than Ca^{2+} clearance by other pathways (Mode 2 CICR), or faster, such that release overwhelms Ca^{2+} clearance, leading to regenerative release (Mode 3 CICR). Do the measurements of J_{pm}, J_{SERCA}, and $P_{ER}(v_i/v_{ER}\kappa_{ER})$ described above help explain these modes of CICR? Although we did not carry out rate measurements at high $[Ca^{2+}]_i$, it is

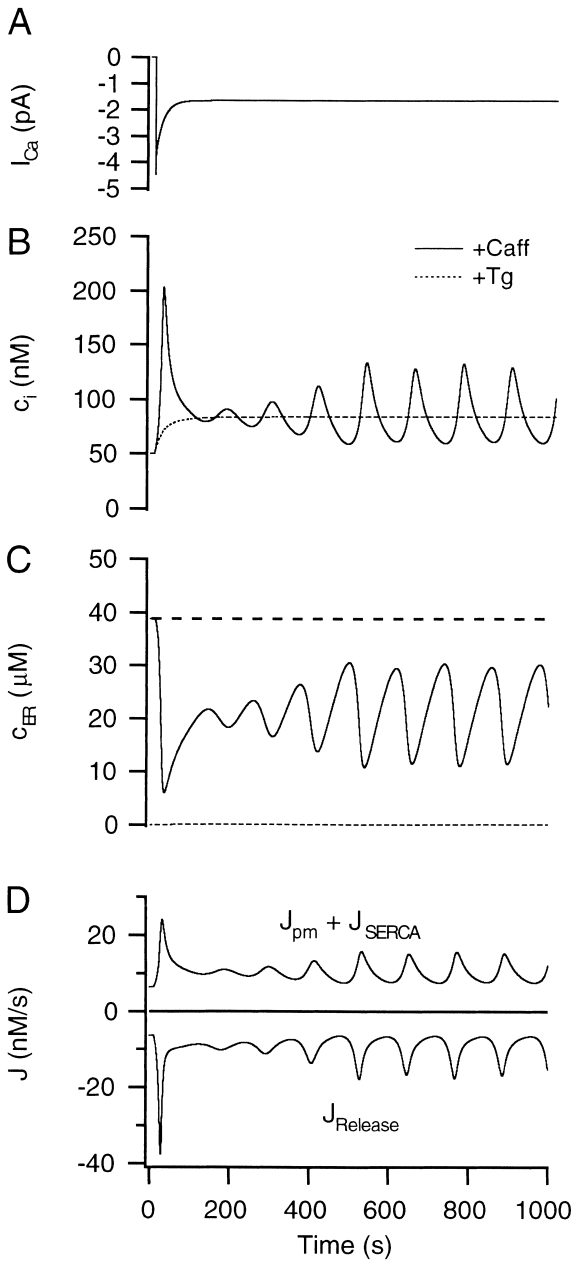

FIGURE 8. Properties of $P_{ER}(v_i/v_{ER}\kappa_{ER})$ in caffeine-treated cells account for steady-state $[Ca^{2+}]_i$ oscillations. (A) I_{Ca} measurement during a 40-s depolarization from −70 to −35 mV that was scaled and extrapolated in time. (B) Comparison between evoked changes in c_i before and after inhibiting ER Ca^{2+} uptake (+Tg). (C) Corresponding changes in c_{ER}. (D) Interplay between Ca^{2+} release ($J_{Release}$) and Ca^{2+} clearance ($J_{Extru} + J_{SERCA}$) during the oscillations. Mitochondrial Ca^{2+} uptake and release were included as described in Colegrove et al. (2000b) to facilitate comparison with responses elicited from unclamped cells by exposure to high K^+. Parameter values were the same as in Fig. 6 (+Caff, +Tg).

possible to investigate the qualitative properties of these modes using the measured rate descriptions extrapolated to higher $[Ca^{2+}]_i$. J_{pm}, J_{SERCA}, and P_{ER} were represented by continuously extending the functions describing their $[Ca^{2+}]_i$ dependence at lower $[Ca^{2+}]_i$ levels. The resulting descriptions coincide with the measured values at low c_i and represent approximations at high c_i. Fig. 9 shows how in the steady state, c_{ER} varies with c_i. When c_i is below ~200 nM, an increase in c_i leads to net Ca^{2+} uptake and a rise in c_{ER}. Increasing c_i further over the physiological range leads to net Ca^{2+}-induced Ca^{2+} release and a decline in c_{ER}. Further (nonphysiological) increases in c_i lead to Ca^{2+} accumulation and a rise in c_{ER}. Thus, there are two major effects of the Ca^{2+} sensitive permeability on the relationship between c_i and c_{ER} under steady-state conditions. First, it leads to the definition of three distinct c_i ranges in which the ER plays qualitatively different roles in Ca^{2+} regulation: low c_i (ER is a Ca^{2+} sink), intermediate c_i (ER is a Ca^{2+} source), and high c_i (ER is a Ca^{2+} sink). Second, it would act as a safety valve to stabilize c_{ER} in the face of prolonged $[Ca^{2+}]_i$ elevations that would otherwise lead to large increases in intraluminal Ca^{2+} levels. With CICR in place, c_{ER} increases by less than a factor of two for a 10,000-fold change in c_i above resting levels.

To illustrate how the Ca^{2+}-sensitive permeability is expected to influence evoked Ca^{2+} signals, Fig. 10 (B and C) shows instantaneous flux/c_i relations like those described in Albrecht et al. (2001), calculated using the same parameter values as in Fig. 9 (with CICR). Fig. 9 A shows the c_i dependence of P_{ER} and $\tilde{P}_{ER}/V_i$, whereas

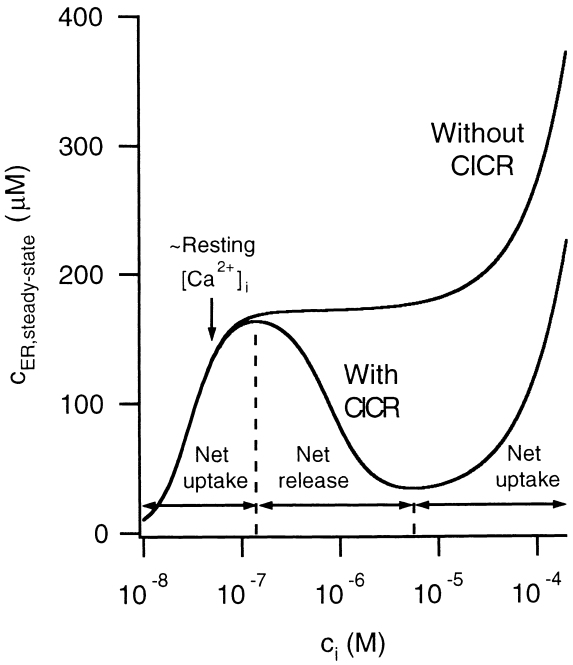

FIGURE 9. Simulated relationship between c_i and c_{ER} under steady-state conditions with and without CICR. J_{SERCA} was described as in Fig. 2 C and $P_{ER}(v_i/v_{ER}\kappa_{ER})$ was described as in Fig. 6 in the control case (with CICR) and +Ryan (without CICR). There are three distinct ranges of c_i: (1) low c_i, where the ER is a Ca^{2+} sink; (2) intermediate c_i, where the ER is a source; and (3) high c_i, where the ER is once again a Ca^{2+} sink. After inhibition of the Ca^{2+}-sensitive permeability, c_{ER} increases monotonically with c_i.

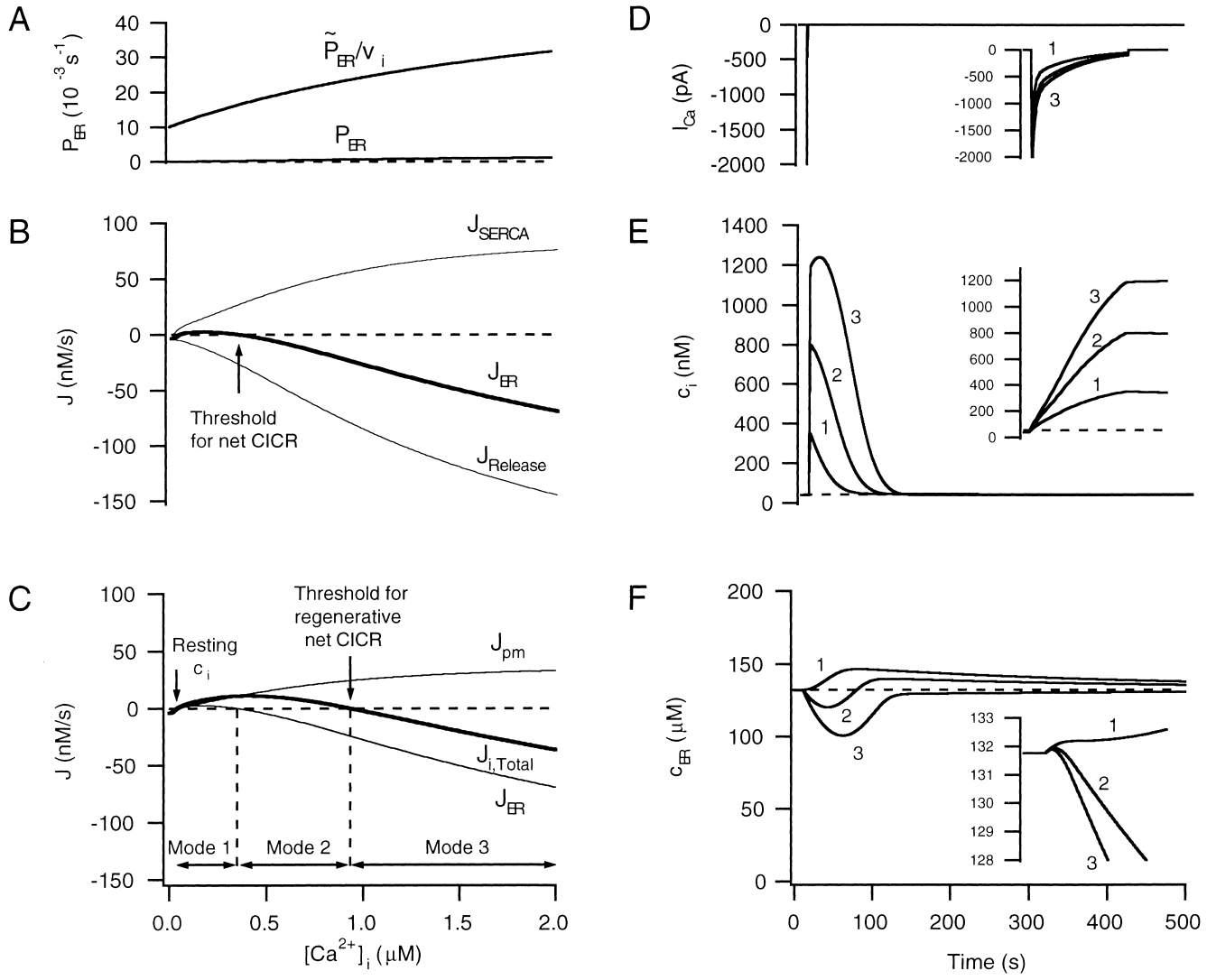

FIGURE 10. Modes of CICR defined by differences in c_i-dependent ER and plasma membrane Ca^{2+} transport. (A) c_I dependence of P_{ER}, and $\tilde{P}_{ER}/v_i$. (B) J_{ER} and its components J_{SERCA} and $J_{Release}$, illustrating the threshold for net CICR (see arrow). (C) c_i dependence of $J_{i,Total}$ and its components J_{ER} and J_{pm}, illustrating the threshold for regenerative CICR (see arrow). Simulations were performed with the same rate descriptions of J_{pm}, J_{SERCA}, and $P_{ER}(v_i/v_{ER}\kappa_{ER})$ as in Fig. 9 assuming that c_{ER} is fixed at its resting value (~132 μM). (D) Ca^{2+} entry waveforms used in the simulations shown in E and F, obtained by scaling a triexponential fit to a measured Ca^{2+} current elicited by a 2-s depolarizing pulse from −70 to −10 mV. (E) c_i responses elicited by the three currents in D. (F) Simulated changes in c_{ER} accompanying the c_i responses shown in D. Insets in E and F compare initial responses to Ca^{2+} entry (D) on the same time axis. Note that stimulus 1 caused ER Ca^{2+} accumulation, but stimuli 2 and 3 caused net Ca^{2+} release; after terminating stimuli 1 and 2, c_i declined, whereas a continued rise occurred after stimulus 3 because c_i exceeded the threshold for regenerative CICR.

Fig. 9 B shows how J_{ER} and its components J_{SERCA} and $J_{Release}$ would be expected to change if c_i was suddenly raised without perturbing c_{ER} from its resting value, assuming a normal resting $[Ca^{2+}]_i$ level (50 nM). When c_i is increased up to ~350 nM, the outward flux J_{SERCA} is larger in magnitude than the inward flux $J_{Release}$, so that the ER accumulates Ca^{2+}. However, Ca^{2+} accumulation becomes gradually slower because of progressive Ca^{2+}-dependent activation of P_{ER}, which we called Mode 1 CICR. When c_i exceeds the threshold for net CICR, $J_{Release}$ is larger in magnitude than J_{SERCA}, causing J_{ER} to be an inward flux, leading to net Ca^{2+} release (Mode 2). The Ca^{2+} level at which this transition occurs, defined by a specific threshold (Fig. 10 B, arrow), depends on the quantitative relationship between the underlying fluxes and their c_i dependence. Similarly, the interplay between Ca^{2+} extrusion across the plasma membrane and net ER Ca^{2+} transport defines the total cytoplasmic Ca^{2+} flux ($J_{i,total}$; Fig. 10 C). When c_i is low, J_{pm} and J_{ER} are both outwardly directed, so that if c_i were increased rapidly to such a level and then allowed to relax, c_i would decline at a rate that is jointly influenced by Ca^{2+} extrusion and net uptake by the ER. If c_i were increased to higher levels where J_{ER} is negative, c_i would also de-

cline, but at a rate that reflects the difference between Ca^{2+} extrusion and net release rates. Finally, if c_i is increased beyond ~935 nM, the rate of net Ca^{2+} release exceeds the rate of Ca^{2+} clearance, leading regenerative release. Fig. 10 (right) illustrates simulated c_i and c_{ER} responses (Fig. 10, E and F) evoked by stimuli that raise c_i to levels below or above the threshold for net Ca^{2+} release, and above the threshold for regenerative net CICR. Simulations were performed using Ca^{2+} entry waveforms obtained from measured Ca^{2+} currents of 2-s duration (Fig. 10 D). As $[Ca^{2+}]_i$ rises during the first (subthreshold) stimulus (curve 1), the ER accumulates Ca^{2+} (Fig. 10 F, inset). After the stimulus ends, c_{ER} continues to rise and c_i declines under the joint influence of Ca^{2+} extrusion across the plasma membrane and Ca^{2+} accumulation by the store. During the second stimulus, which exceeds the threshold for net CICR (curve 2), the ER is transformed into a source, with c_{ER} eventually declining below the basal level (Fig. 10 F, inset). When the stimulus ends, c_i declines initially at a rate that depends on Ca^{2+} extrusion and net Ca^{2+} release, but the recovery is eventually accelerated when the ER once again becomes a Ca^{2+} sink, causing an overshoot of the basal level before c_{ER} finally approaches the resting value. The third stimulus (curve 3) is sufficiently strong to bring c_i above the threshold for regenerative CICR, such that when the stimulus ends, c_i continues to rise under the influence of continued net Ca^{2+} release at a rate that exceeds the rate of Ca^{2+} extrusion. Thus, the extrapolated rate descriptions for J_{pm}, J_{SERCA}, and P_{ER} provide an explanation for the observation that stimuli producing progressively larger $[Ca^{2+}]_i$ elevations cause the ER to undergo a transition from sink to source (Hongpaisan et al., 2001).

DISCUSSION

The main goal of this study was to determine how Ca^{2+}-dependent activation of a ryanodine-sensitive CICR pathway contributes to $[Ca^{2+}]$ responses evoked by weak depolarization. Our previous study showed that under these conditions of stimulation, the ER accumulates Ca^{2+}, but we also presented indirect evidence that the rate of Ca^{2+} accumulation is attenuated by activation of the CICR pathway, which, in effect, makes the ER a weaker Ca^{2+} buffer. Since the rate of net ER Ca^{2+} transport depends on the relative rates of Ca^{2+} uptake and release via different transport pathways, we characterized these rates and their regulation by Ca^{2+} to test the hypothesis that the direction and rate of net ER Ca^{2+} transport depends on a slight imbalance between uptake and release rates of much larger magnitude, each showing a distinct functional dependence on $[Ca^{2+}]$. We found that Ca^{2+} uptake is regulated by SERCAs in a $[Ca^{2+}]_i$-dependent manner, and that passive Ca^{2+} release is regulated by a $[Ca^{2+}]_i$-sensitive permeability that is modified by caffeine and ryanodine in a way that indicates it is dominated by ryanodine-sensitive Ca^{2+} release channels. It was found that quantitative differences in the $[Ca^{2+}]_i$ sensitivity of Ca^{2+} uptake and release rates account for Mode 1 CICR. Although these rates are in balance under resting conditions, small $[Ca^{2+}]_i$ elevations stimulate Ca^{2+} uptake more strongly than Ca^{2+} release, accounting for Ca^{2+} accumulation. Moreover, increases in the rate of passive Ca^{2+} release by such small $[Ca^{2+}]_i$ elevations, reflecting a $[Ca^{2+}]_i$-induced rise in ER Ca^{2+} permeability, reduces the imbalance between uptake and release rates, accounting for attenuated Ca^{2+} accumulation during stimulation. Taken together with the properties of Ca^{2+} extrusion across the plasma membrane, these same transport pathways account for caffeine-induced $[Ca^{2+}]_i$ oscillations. Finally, extending the rate descriptions of Ca^{2+} uptake and release to higher $[Ca^{2+}]_i$ levels provides an explanation for our finding that as depolarization-evoked $[Ca^{2+}]_i$ elevations become larger, the ER becomes a less effective Ca^{2+} buffer, and at high $[Ca^{2+}]_i$, becomes a Ca^{2+} source.

Properties of the ER Ca^{2+} Uptake Pathway

The impact of SERCAs (J_{SERCA}) on Ca^{2+} dynamics was assessed by measuring the t-BuBHQ-sensitive component of the total cytoplasmic Ca^{2+} flux (J_i) just after exposing cells to a high concentration of t-BuBHQ. As it was measured, the $[Ca^{2+}]_i$ dependence of J_{SERCA} is expected to depend both on the rate of Ca^{2+} uptake via SERCAs at the instant of inhibition, and the properties of cytoplasmic Ca^{2+} buffering. The composite $[Ca^{2+}]_i$ dependence of J_{SERCA} could be described by Eq. B8 quite well, and along with the other transport characterizations it made it possible to reconstruct the observed t-BuBHQ-induced $[Ca^{2+}]_i$ transients. While the equations used to describe transport in this study were mechanistically motivated, they should be regarded as empirical descriptions of the transport rates and their $[Ca^{2+}]_i$ dependence. Nevertheless, it is noteworthy that the apparent $[Ca^{2+}]_i$ sensitivity of uptake ($EC_{50,SERCA} <$ 100 nM) was higher than expected based on studies of SERCAs in isolation (Lytton et al., 1992). One possible explanation is that CICR raises local $[Ca^{2+}]_i$ beyond the level detected by bulk $[Ca^{2+}]_i$ measurements. Such an increase could partially saturate the uptake pathway, even though bulk $[Ca^{2+}]_i$ is considerably lower. As shown by Albrecht et al. (2001), ryanodine does not alter J_{SERCA} under resting conditions, arguing against such an effect when $[Ca^{2+}]_i$ is at its resting level. However, with stronger activation of the CICR pathway at higher $[Ca^{2+}]_i$, it is possible that increases in local $[Ca^{2+}]_i$ near sites of ER Ca^{2+} uptake bring SERCAs close to saturation, so that at high $[Ca^{2+}]_i$ the $[Ca^{2+}]_i$ dependence of J_{SERCA} largely reflects the $[Ca^{2+}]_i$ depen-

dence of κ_i. Assessment of this possibility will require additional information regarding the spatial distribution of Ca^{2+} near the ER and the specific SERCA isoforms that are expressed in sympathetic neurons.

Characterization of the Ca^{2+} Permeability of the ER

It has been difficult to characterize CICR in intact cells because the rate of passive Ca^{2+} release depends on two factors that are difficult to distinguish experimentally in intact cells: driving force and permeability. It is expected that Ca^{2+} release channel activity influences $J_{Release}$ primarily through its effect on P_{ER}, and secondarily through its effect on driving force; although the latter effect depends on other transport systems that influence ER Ca^{2+} loading, such as Ca^{2+} uptake and extrusion. We devised a way to distinguish between these contributions to $J_{Release}$. Integration of $J_{Release}\kappa_i$ provided a measure of changes in intraluminal Ca^{2+} concentration, which in turn made it possible to estimate the driving force for Ca^{2+} release. Along with the definition of P_{ER} provided by Eq. 4, this made it possible to obtain a quantity that is expected to be proportional to the macroscopic permeability of the ER ($\tilde{P}_{ER}$) from the ratio of two measured quantities.

Based on this procedure, we characterized $\tilde{P}_{ER}$ and its $[Ca^{2+}]$ dependence, as well as its sensitivity to pharmacological agents known to modify RyR gating in vitro. We found that (1) $\tilde{P}_{ER}/(v_{ER}\kappa_{ER})$ increases with $[Ca^{2+}]_i$ over the range studied (up to ~250 nM), which is consistent with regulation of RyR activity through low affinity Ca^{2+}–channel interactions with little cooperativity. (2) Caffeine increased, and ryanodine reduced, the $[Ca^{2+}]_i$ sensitivity of $\tilde{P}_{ER}/(v_{ER}\kappa_{ER})$, arguing that its $[Ca^{2+}]_i$ dependence is dominated by RyRs. The apparent loss of Ca^{2+} sensitivity after ryanodine treatment also provides a simple explanation for the previous finding that ryanodine enhances ER Ca^{2+} accumulation during depolarization. By preventing a Ca^{2+}-dependent increase in ER Ca^{2+} permeability, ryanodine also prevents an increase in the rate of Ca^{2+} release that normally occurs in response to evoked elevations in $[Ca^{2+}]_i$. This would exaggerate the imbalance between uptake and release rates under conditions where the ER is a Ca^{2+} sink, rendering the ER a more powerful Ca^{2+} buffer. (3) Ryanodine increased basal $\tilde{P}_{ER}/(v_{ER}\kappa_{ER})$, which is consistent with its effects on RyR open probability at the concentration used (1 μM). This result provides an explanation for our finding that ryanodine at the same concentration reduces basal intraluminal total Ca concentration (and presumably free Ca concentration) without altering the basal rate of Ca^{2+} uptake or release (Albrecht et al., 2001). (4) The $[Ca^{2+}]_I$ dependence of $\tilde{P}_{ER}/(v_{ER}\kappa_{ER})$ was not detectably different during the rising and falling phases of the t-BuBHQ-induced $[Ca^{2+}]_i$ transients.

This leads to two conclusions about RyR regulation during these responses. First, $\tilde{P}_{ER}$ is not very sensitive to reductions in intraluminal Ca^{2+} concentration that occur during these two phases of the transients. In other words, the major sites responsible for Ca^{2+}-dependent regulation of $\tilde{P}_{ER}$ are directly accessible from the cytoplasmic solution. This agrees with the conclusions of Xu and Meissner (1998), who showed that intraluminal Ca levels influence gating of canine cardiac RyRs in a way that can be accounted for by Ca^{2+} release followed by interactions with cytoplasmic regulatory sites. Second, $\tilde{P}_{ER}$ does not show appreciable intrinsic time dependence. This finding is consistent with the results of Schiefer et al. (1995) who showed there is little inactivation of canine cardiac RyRs when cis $[Ca^{2+}] < 1$ μM (our measurements of $\tilde{P}_{ER}$ were made below 250 nM). Thus, the effects of caffeine and ryanodine on $\tilde{P}_{ER}$ at low $[Ca^{2+}]_i$ are in general agreement with in vitro studies of RyRs derived from mammalian cardiac cells.

Assumptions Used in the Analysis

An important step in characterizing $\tilde{P}_{ER}$ was estimation of the driving force for passive Ca^{2+} release. Several approximations were made. First, it was assumed that the ER membrane potential is small enough that it has little or no effect on $J_{Release}$. Second, it was assumed that intraluminal Ca^{2+} buffers bind Ca^{2+} rapidly and with low affinity. Third, it was assumed that $\Delta[Ca^{2+}]_i$ is small enough compared with $\Delta[Ca^{2+}]_{ER}$ (the differences between $[Ca^{2+}]_i$ and $[Ca^{2+}]_{ER}$ and their basal levels during t-BuBHQ-induced $[Ca^{2+}]_i$ transients) that cytoplasmic Ca^{2+} has negligible effect on driving force (APPENDIX A).

Our results describe the quantitative properties of ER Ca^{2+} transport in intact cells under conditions where the spatial distribution of Ca^{2+} within cellular compartments is likely to be nearly uniform. How relevant are the rate descriptions obtained under these conditions to the case where Ca^{2+} is distributed nonuniformly (e.g., during depolarization-evoked Ca^{2+} entry)? In this case, $[Ca^{2+}]_i$ is highest near sites of Ca^{2+} entry and falls off with distance from the plasma membrane (Sala and Hernandez-Cruz, 1990; Hua et al., 1993). As long as the transport descriptions refer to populations of Ca^{2+} transporters that are distributed uniformly within the membranes delimiting compartments, and these membranes have simple geometry, the results are also expected to predict the spatial distribution of $[Ca^{2+}]$ within compartments during periods of Ca^{2+} entry. Results that support this conclusion have been presented for the analogous problem of mitochondrial Ca^{2+} loading during depolarization (Pivovarova et al., 1999). Moreover, examination of the case where Ca^{2+} is spatially uniform provides an explanation for the basis of steady-state Ca^{2+} level within ER in terms of the quantitative properties of ER Ca^{2+} uptake and release rates,

and shows how $[Ca^{2+}]_i$ levels help determine which modes of CICR can be recruited in response to stimulation. Nevertheless, if the distribution of the ER or of transporters within ER or plasma membranes is nonuniform, for example, such that the density or intrinsic properties of ER transporters vary appreciably from one somatic region to another (e.g., peripheral versus central regions), or if proximity between intracellular membranes permits the development of Ca^{2+} microdomains (Rizzuto et al., 1998), an accurate description of $[Ca^{2+}]$ dynamics during stimulation would require detailed specification of the distribution of transporters and membrane geometry. An example where spatial nonuniformity may introduce an error in the $[Ca^{2+}]_i$ dependence of transport presented in this study was mentioned in connection with J_{SERCA}.

Comparison with Previous Work

To our knowledge, this is the first description of ER Ca^{2+} uptake and release fluxes and Ca^{2+} permeability in intact cells. Our study builds on previous work in skeletal (Baylor et al., 1983; Kovacs et al., 1983; Melzer et al., 1987) and cardiac muscle (Sipido and Wier, 1991) describing CICR from the SR after membrane depolarization. As in these studies, we used the basic idea that at each instant in time, $[Ca^{2+}]_i$ changes at a rate that depends on the rates of passive Ca^{2+} release and removal, and on the properties of intracellular Ca^{2+} buffering. Thus, with information about the rate of Ca^{2+} removal and buffering, the rate of Ca^{2+} release can be calculated from the total Ca^{2+} flux. In these earlier studies, the rate of Ca^{2+} uptake was not measured, and was either included in an overall description of Ca^{2+} removal (Melzer et al., 1987) or was calculated (Sipido and Wier, 1991). In the present study, we used t-BuBHQ as a tool to measure both the rates of ER Ca^{2+} uptake and release and their $[Ca^{2+}]$ dependence. As a result, it was possible to describe the relationship between Ca^{2+} uptake and release fluxes during and after stimulation, which was essential for understanding the direction and rate of net ER Ca^{2+} transport during depolarization and how it is regulated by $[Ca^{2+}]_i$. With an understanding of the basis of net ER Ca^{2+} transport, it became possible to clarify how the interplay between net ER Ca^{2+} transport and Ca^{2+} extrusion across the plasma membrane sets the stage for multiple modes of CICR.

Caffeine-induced Ca^{2+} Oscillations

Previous studies have shown that when sympathetic neurons are exposed steadily to caffeine and then depolarized, $[Ca^{2+}]_i$ oscillates (Lipscombe et al., 1988; Friel and Tsien, 1992b; Kuba, 1994). Oscillations can be elicited by caffeine alone, but in our experiments, depolarization considerably increased the reliability with which they are evoked. In an earlier study (Friel, 1995), three independent components of the total Ca^{2+} flux underlying caffeine-induced Ca^{2+} oscillation were measured. These components represented caffeine-sensitive Ca^{2+} release, Ca^{2+} entry, and the remainder of the total cytoplasmic Ca^{2+} flux, interpreted as the sum of the rates of Ca^{2+} extrusion and Ca^{2+} uptake. A simple model was presented that accounted for small amplitude oscillations when $[Ca^{2+}]_i$ was low enough that mitochondrial Ca^{2+} transport was weak and linear approximations of the $[Ca^{2+}]_i$ dependence of Ca^{2+} extrusion and uptake are adequate. In this model, the rate of Ca^{2+} release was described as a product of a permeability factor and a driving force, as in the present study. The permeability was assumed to increase monotonically with $[Ca^{2+}]_i$, was insensitive to intraluminal Ca^{2+} concentration and did not show inactivation.

In the present study, this permeability was directly characterized and the third component of the total cytoplasmic Ca^{2+} flux was explicitly represented by the sum of two fluxes J_{SERCA} and J_{pm} that were measured in the absence of caffeine under conditions where $[Ca^{2+}]_i$ is not oscillating. It is remarkable that simulations performed using descriptions of J_{pm}, J_{SERCA}, and κ_i from control cells, and of P_{ER} from each of the four caffeine-treated cells, showed $[Ca^{2+}]_i$ oscillations in response to stimulated Ca^{2+} entry, whereas descriptions from the same number of control cells did not. It was possible to reproduce the basic properties of $[Ca^{2+}]_i$ oscillations evoked by stimulated Ca^{2+} entry, as well as the temporal properties of the three flux components measured in the earlier study (Fig. 7).

Importance of Studying Ca^{2+} Regulation by the Collection of Transporters Expressed together in Intact Cells

Studies from various in vitro preparations (e.g., vesicles, and isolated organelles) has provided information regarding the types of transporters that participate in Ca^{2+} signaling and their biophysical properties. However, since this information is derived from multiple tissues and species, it may not describe the particular collection of transporters that operate together in any one cell type. Such in vitro data have been invaluable in developing general concepts about Ca^{2+} regulation, but inferences drawn from them are limited. One reason is that the Ca^{2+} transport rates depend on $[Ca^{2+}]$ in a nonlinear manner. In a coupled system of nonlinear Ca^{2+} transporters, quantitative properties of the individual transport systems can influence qualitative properties of Ca^{2+} regulation. Therefore, to understand the Ca^{2+} signaling regimes that can exist in vivo, it is necessary to consider collections of transporters that are actually expressed together in living cells.

Our results show that the relative rates of ER Ca^{2+} uptake and release are critical in determining whether depolarization-evoked $[Ca^{2+}]_i$ elevations lead to ER Ca^{2+}

accumulation or net Ca^{2+} release, and, therefore, whether intraluminal Ca^{2+} concentrations rise or fall in response to stimulation. The relative rates of transport are expected to depend on multiple factors, including transporter expression levels, sensitivity to Ca^{2+}, and the state of modulation. Differences between the relative rates of Ca^{2+} uptake and release in vivo and those deduced from in vitro data could lead to completely different predictions regarding the direction in which ER Ca^{2+} concentrations change in response to particular stimuli. Certainly, from the standpoint of regulation of intraluminal Ca^{2+} sensors, this is an important difference.

Implications for Studies of Ca^{2+} Signaling

Our results provide a picture of CICR in intact cells in terms of the interplay between multiple transport systems that can lead to qualitatively different modes of Ca^{2+} dynamics in response to different patterns of stimulated Ca^{2+} entry. One approach illustrating this was in terms of instantaneous flux/c_i relations analogous to the momentary current voltage relations used previously to illustrate the basis for initial responses to depolarizing stimuli in excitable cells (Jack et al., 1983). We described how $[Ca^{2+}]_i$ and $[Ca^{2+}]_{ER}$ would be expected to change after an increase in $[Ca^{2+}]_i$ that was so rapid that changes in $[Ca^{2+}]_{ER}$ would be negligible. Although useful for describing qualitative properties of Ca^{2+} dynamics, the instantaneous flux/c_i relations shown in Fig. 10 do not show how the properties of CICR change during stimulation in response to changes in intraluminal Ca^{2+} concentration. However, these changes can be predicted for arbitrary stimuli using the rate descriptions presented in this study. For example, one conclusion is that ER Ca^{2+} (accumulation/net release) should (lower/raise) the threshold for net CICR as a consequence of changes in driving force of passive Ca^{2+} release. As a result, which mode of CICR that is recruited during stimulation would depend critically on the history of stimulation.

Regarding the role of mitochondria, the rate descriptions of J_{pm}, J_{SERCA}, and $\tilde{P}_{ER}$ were obtained under conditions where mitochondrial Ca^{2+} uptake is weak, but also are expected to apply when mitochondrial Ca^{2+} transport is strong. Indeed, after including rate descriptions for mitochondrial Ca^{2+} uptake and release, obtained in cells where ER Ca^{2+} transport was inhibited, it was possible to reproduce most of the features of $[Ca^{2+}]_i$ elevations evoked under voltage clamp and of caffeine-induced $[Ca^{2+}]_i$ oscillations. As argued in Albrecht et al. (2001) and Hongpaisan et al. (2001), Ca^{2+} transport by mitochondria is also expected to influence the prevailing mode of CICR indirectly by modulating $[Ca^{2+}]_i$.

In addition to establishing three different $[Ca^{2+}]_i$ ranges supporting different modes of CICR during stimulation, the presence of a CICR pathway also stabilizes intraluminal Ca^{2+} concentrations over a wide range of $[Ca^{2+}]_i$. This may be important in maintaining processes that are sensitive to intraluminal Ca^{2+} levels (Meldolesi and Pozzan, 1998; Corbett and Michalak, 2000) in the face of large swings in $[Ca^{2+}]_i$ that might occur in response to excessive stimulation or injury.

APPENDIX A

Assessment of ER Ca^{2+} Permeability in Intact Cells

The purpose of this appendix is to derive an equation that relates the macroscopic Ca^{2+} permeability of the ER ($\tilde{P}_{ER}$) to measurements in intact cells presented in this study. Let $\tilde{J}_{ER}$ be the rate of net Ca^{2+} transport between the ER and cytoplasm (e.g., in units of nmol/s). This flux would cause the total ER Ca concentration ($[Ca]_{ER}$) to change at a rate given by Eq. A1:

$$\frac{d[Ca]_{ER}}{dt} = \frac{\tilde{J}_{ER}}{v_{ER}}, \tag{A1}$$

where v_{ER} is the ER volume and outward fluxes from the cytoplasm are positive and inward fluxes are negative. For simplicity, it is assumed that Ca^{2+} is uniformly distributed within the ER and cytoplasm at all times, which is a reasonable approximation as long as transport between compartments is slow compared with diffusion within compartments. If binding to intraluminal Ca^{2+} buffers reaches equilibrium rapidly, then this flux would cause the intraluminal free Ca^{2+} concentration ($[Ca^{2+}]_{ER}$) to change at a rate of

$$\frac{d[Ca^{2+}]_{ER}}{dt} = \frac{\tilde{J}_{ER}}{v_{ER}\kappa_{ER}}, \tag{A2}$$

where κ_{ER} is the ratio of change in total ER Ca concentration to the accompanying change in free Ca concentration. In the absence of other forms of net cytoplasmic Ca^{2+} transport, the same flux would cause the cytoplasmic free Ca^{2+} concentration to change at a rate given by Eq. A3:

$$\frac{d[Ca^{2+}]_i}{dt} = -\frac{\tilde{J}_{ER}}{v_i\kappa_i} \equiv -J_{ER}, \tag{A3}$$

where J_{ER} can be interpreted as the net flux (e.g., in units nmol/liter s) of Ca^{2+} between the ER and cytoplasm per unit effective cytoplasmic volume ($v_i\kappa_i$; Melzer et al., 1987). J_{ER} can be separated into two components:

$$J_{ER} = J_{SERCA} + J_{Release}, \tag{A4}$$

where J_{SERCA} represents Ca^{2+} uptake via SERCAs, and $J_{Release}$ represents passive Ca^{2+} release. Results presented in Fig. 2 provide information about J_{SERCA}, whereas Figs. 3 and 4 show measurements of $J_{Release}$.

$J_{Release}$ is expected to depend both on the Ca^{2+} permeability of ER and the driving force for Ca^{2+} movement across the ER membrane. If this driving force depends only on the difference between cytoplasmic and intraluminal Ca^{2+} concentrations, $J_{Release}$ can be described at each point in time as follows:

$$\begin{aligned} J_{Release} &= \frac{\tilde{J}_{Release}}{v_i \kappa_i} \\ &= \frac{\tilde{P}_{ER}}{v_i \kappa_i}([Ca^{2+}]_i - [Ca^{2+}]_{ER}) \\ &= P_{ER}([Ca^{2+}]_i - [Ca^{2+}]_{ER}), \end{aligned} \tag{A5}$$

where $\tilde{P}_{ER}$ is the permeability of the entire ER membrane (units $cm^3 s^{-1}$) and $P_{ER} = \tilde{P}_{ER}/v_i\kappa_i$ (in units s^{-1}). $\tilde{P}_{ER}$ is a macroscopic permeability that can be related to single-channel properties by $\tilde{P}_{ER} = \Sigma_u N_u p_u \pi_u$, where N_u is the number of Ca^{2+}-permeable channels of type u, p_u is their open probability, and π_u is the unitary Ca^{2+} permeability, if permeation through channels is the dominant form of passive ER Ca^{2+} transport. Note that if a channel contributing to $\tilde{P}_{ER}$ has a $[Ca^{2+}]_i$-dependent open probability (e.g., RyRs), then $\tilde{P}_{ER}$ will depend on $[Ca^{2+}]_i$. Eq. A5 can be rewritten as follows:

$$\begin{aligned} J_{Release}(t) &= P_{ER}\{([Ca^{2+}]_i(t) - [Ca^{2+}]_{i,basal}) - \\ &\quad ([Ca^{2+}]_{ER}(t) - [Ca^{2+}]_{ER,basal}) + \\ &\quad ([Ca^{2+}]_{i,basal} - [Ca^{2+}]_{ER,basal})\} \\ &= P_{ER}\{\Delta[Ca^{2+}]_i(t) - \Delta[Ca^{2+}]_{ER}(t) + \\ &\quad ([Ca^{2+}]_{i,basal} - [Ca^{2+}]_{ER,basal})\} \end{aligned} \tag{A6}$$

where $\Delta[Ca^{2+}]_i(t)$ and $\Delta[Ca^{2+}]_{ER}(t)$ are the differences between $[Ca^{2+}]_i$ and $[Ca^{2+}]_{ER}$ at time t and their basal values after inhibition of SERCAs (e.g., with t-BuBHQ). If in the continuous presence of t-BuBHQ, Ca^{2+} becomes passively distributed between the ER and cytoplasm, then $[Ca^{2+}]_{ER,basal} = [Ca^{2+}]_{i,basal}$ and Eq. A6 reduces to

$$J_{Release}(t) = P_{ER}(\Delta[Ca^{2+}]_i(t) - \Delta[Ca^{2+}]_{ER}(t)). \tag{A7}$$

Now, if $\Delta[Ca^{2+}]_i(t) \ll \Delta[Ca^{2+}]_{ER}(t)$, Eq. A7 can be approximated by

$$J_{Release}(t) \approx -P_{ER}\Delta[Ca^{2+}]_{ER}(t). \tag{A8}$$

To obtain $\Delta[Ca^{2+}]_{ER}(t)$, Eq. A2 can be integrated from the instant of SERCA inhibition to the time t and then offset by the integral over the entire t-BuBHQ-induced $[Ca^{2+}]_i$ transient:

$$\begin{aligned} \Delta[Ca^{2+}]_{ER}(t) &= \int_0^t \frac{d[Ca^{2+}]_{ER}}{dt}dt' - \int_0^\infty \frac{d[Ca^{2+}]_{ER}}{dt}dt' \\ &= -\int_t^\infty \frac{d[Ca^{2+}]_{ER}}{dt}dt' \\ &= -\int_t^\infty \frac{\tilde{J}_{ER}}{v_{ER}\kappa_{ER}}dt' \\ &= -\int_t^\infty \frac{\tilde{J}_{ER}}{v_i\kappa_i}\frac{v_i\kappa_i}{v_{ER}\kappa_{ER}}dt. \end{aligned} \tag{A9}$$

If inhibition of Ca^{2+} uptake is complete, $J_{SERCA} = 0$, and so from Eqs. A3 and A4 $J_{ER} = J_{Release}$, $\tilde{J}_{ER}/(v_i\kappa_i) = J_{Release}$, so that Eq. A9 becomes:

$$\Delta[Ca^{2+}]_{ER}(t) = -\int_t^\infty J_{Release}\frac{v_i\kappa_i}{v_{ER}\kappa_{ER}}dt'. \tag{A10}$$

If v_i/v_{ER} and κ_{ER} do not change with time during the t-BuBHQ-induced $[Ca^{2+}]_i$ transients, then Eq. A10 can be written:

$$\begin{aligned} \Delta[Ca^{2+}]_{ER}(t) &= -\frac{v_i}{v_{ER}\kappa_{ER}}\int_t^\infty J_{Release}\kappa_i dt' \\ &= \frac{v_i}{v_{ER}\kappa_{ER}}\Delta[Ca^{2+}]^{(i)}_{ER}(t), \end{aligned} \tag{A11}$$

where $\Delta[Ca^{2+}]^{(i)}_{ER}(t)$ designates minus one times the integral and can be interpreted as the change in total Ca concentration that would occur if the net ER Ca^{2+} flux from t onward were deposited in a closed compartment having the same volume as the cytoplasm. κ_i is retained under the integral sign to allow for changes in cytoplasmic Ca^{2+} strength that occur as $[Ca^{2+}]_i$ changes with time (Fig. 1 D). However, it is assumed that κ_i adjusts instantaneously to changes in $[Ca^{2+}]_i$, so that if it varies with time, it derives its time dependence exclusively from the time dependence of $[Ca^{2+}]_i$. Substituting the expression for $\Delta[Ca^{2+}]_{ER}(t)$ (Eq. A11) into Eq. A8 gives:

$$J_{Release}(t) \approx -\frac{P_{ER}v_i}{v_{ER}\kappa_{ER}}\Delta[Ca^{2+}]^{(i)}_{ER}(t). \tag{A12}$$

Eq. A12 makes it possible to define a function related to permeability in terms of measured quantities:

$$\frac{P_{ER}v_i}{v_{ER}\kappa_{ER}} \approx -\frac{J_{Release}(t)}{\Delta[Ca^{2+}]^{(i)}_{ER}(t)}. \tag{A13}$$

(See Shirokova et al., 1995, for an alternative approach to measuring SR Ca^{2+} permeability in skeletal muscle.) This can be related to the macroscopic permeability of the ER ($\tilde{P}_{ER}$) by Eq. A14:

$$\begin{aligned} \frac{P_{ER}v_i}{v_{ER}\kappa_{ER}} &= \left[\frac{\tilde{P}_{ER}}{v_i\kappa_i}\right]\frac{v_i}{v_{ER}\kappa_{ER}} \\ &= \left[\frac{1}{\kappa_i}\right]\frac{\tilde{P}_{ER}}{v_{ER}\kappa_{ER}}. \end{aligned} \tag{A14}$$

Therefore, if $v_{ER}\kappa_{ER}$ is constant, $P_{ER}(v_i/v_{ER}\kappa_{ER})$ is expected to show a composite $[Ca^{2+}]_i$ dependence reflecting both the properties of κ_i and $\tilde{P}_{ER}$. In this study, we present measurements of $P_{ER}(v_i/v_{ER}\kappa_{ER})$ to avoid assumptions regarding $(v_i/v_{ER}\kappa_{ER})$. Multiplication by κ_i using results shown in Fig. 1 D then gives $\tilde{P}_{ER}/(v_{ER}\kappa_{ER})$. If $v_{ER}\kappa_{ER}$ is constant, this is proportional to the macroscopic Ca^{2+} permeability of the ER. Given measurements of $\Delta[Ca^{2+}]^{(i)}_{ER}(t)$, estimates of $\Delta[Ca^{2+}]_{ER}(t)$ are obtained after multiplying by $(v_i/v_{ER}\kappa_{ER})$.

The validity of Eq. A13 depends on the approximation $\Delta[Ca^{2+}]_i(t) - \Delta[Ca^{2+}]_{ER}(t) \approx -\Delta[Ca^{2+}]_{ER}(t)$ used in obtaining Eq. A8 from Eq. A7. If during evoked t-BuBHQ transients $\Delta[Ca^{2+}]_i(t) < 250$ nM and $\Delta[Ca^{2+}]_{ER}(t) > 25$ μM, the error in estimating $P_{ER}(v_i/v_{ER}\kappa_{ER})$ would be ~1% and would be smaller when $\Delta[Ca^{2+}]_{ER}(t)$ is higher. During the final phase of the recovery, $-\Delta[Ca^{2+}]_{ER}(t)$ systematically overestimates $(\Delta[Ca^{2+}]_i(t) - \Delta[Ca^{2+}]_{ER}(t))$ in magnitude, leading to an underestimation of $P_{ER}(v_i/v_{ER}\kappa_{ER})$. However, such an underestimation was difficult to resolve (Fig. 3 E, light trace) possibly because in this case $P_{ER}(v_i/v_{ER}\kappa_{ER})$ is determined from the ratio of two small and noisy numbers.

APPENDIX B

Description of the Model

The dynamics of the free Ca^{2+} concentration within the cytosol (c_i) and the ER (c_{ER}) were represented by the following differential equations (Eqs. B1 and B2):

$$\frac{dc_i}{dt} = -J_i \tag{B1}$$

$$\frac{dc_{ER}}{dt} = J_{ER}\frac{v_i\kappa_i}{v_{ER}\kappa_{ER}}, \tag{B2}$$

where the total cytoplasmic Ca^{2+} flux is given by Eq. B3

$$J_i = J_{pm} + J_{ER}, \tag{B3}$$

and the intercompartmental fluxes J_{pm} and J_{ER} depend on the relative rates of transport via different pathways as follows:

$$J_{pm} = J_{extru} + J_{ICa}, \tag{B4}$$

and

$$J_{ER} = J_{SERCA} + J_{Release}, \tag{B5}$$

where

$$J_{extru} = \left\{k_{leak,pm}(c_i - c_o) + \frac{V_{max,extru}}{\left[1 + \left(\frac{EC_{50,extru}}{c_i}\right)^{n_{extru}}\right]}\right\}\kappa_i^{-1} \tag{B6}$$

$$J_{ICa} = \frac{I_{Ca}}{2Fv_i\kappa_i}, \tag{B7}$$

$$J_{SERCA} = \frac{V_{max,SERCA}}{\kappa_i\left[1 + \left(\frac{EC_{50,SERCA}}{c_i}\right)^{n_{SERCA}}\right]}, \tag{B8}$$

$$J_{Release} = \frac{\tilde{P}_{ER}(c_i - c_{ER})}{v_i\kappa_i}, \tag{B9}$$

and

$$\frac{\tilde{P}_{ER}}{v_i} = \tilde{P}_{basal} + \frac{\tilde{P}_{max,RyR}}{\left[1 + \left(\frac{EC_{50,RYR}}{c_i}\right)^{n_{RyR}}\right]}, \tag{B10}$$

where $k_{leak,pm}$, c_o, $V_{max,extru}$, $EC_{50,extru}$, n_{extru}, F, $V_{max,SERCA}$, $EC_{50,SERCA}$, n_{SERCA}, $\tilde{P}_{basal}$, $\tilde{P}_{max,RyR}$, $EC_{50,RyR}$, and n_{RyR} are constants. c_o is the extracellular Ca^{2+} concentration and F is the Faraday constant. Eqs. B4–B9 describe the rate of total Ca^{2+} transport by the respective pathways divided by the cytoplasmic volume (v_i) and the cytoplasmic buffering factor κ_i. According to the sign convention used, fluxes that raise c_i are negative while fluxes that lower c_i are positive. J_{extru} is the sum of plasma membrane pump and leak fluxes. $\tilde{P}_{ER}/v_i$, a lumped quantity representing the total ER permeability per unit cytoplasmic volume, consists of a constant basal component ($\tilde{P}_{basal}$) and a c_i-dependent component that increases saturably with c_i (half-maximal activation when $c_i = EC_{50,RyR}$) and approaches $\tilde{P}_{max,RyR}$ when is high c_i.

To obtain an analytical description of ER Ca^{2+} permeability for use in simulations, measurements of $P_{ER}(v_i/v_{ER}\kappa_{ER})$ were described by Eq. B11:

$$\frac{P_{ER}v_i}{v_{ER}\kappa_{ER}} = \left[\frac{1}{\kappa_i}\right]\left[\frac{\tilde{P}_{ER}}{v_i}\right]\left[\frac{v_i}{v_{ER}\kappa_{ER}}\right], \tag{B11}$$

where κ_i was treated as a known function of $[Ca^{2+}]_i$ based on measurements shown in Fig. 1 D, $(\tilde{P}_{ER}/v_i)$ was described by Eq. B10, $v_{ER}\kappa_{ER}/v_i$ was estimated to be unity. The description of mitochondrial Ca^{2+} transport used in simulations (Figs. 6–8) is from Colegrove et al. (2000b).

In carrying out simulations, the resting value of c_i was determined as the solution of Eq. B6 when $J_{pm} = 0$. Alternatively, if simulations were to be compared at the same value of resting c_i, (Fig. 5, A and B, insets), Eq. B6 was solved determine the value of $k_{leak,pm}$ yielding that value of c_i. The initial value of c_{ER} was determined as the particular level where Ca^{2+} uptake and release rates are equal at the prevailing basal c_i according to Eq. B12:

$$c_{ER}(0) = c_i(0) + \frac{J_{SERCA}(c_i(0))}{\tilde{P}_{ER}(c_i(0))/v_i}. \tag{B12}$$

Therefore, at rest c_{ER} is defined by the properties of J_{SERCA} and $\tilde{P}_{ER}/v_i$ and basal c_i.

The authors thank Drs. Hillel Chiel and Steve Jones for their helpful comments on the manuscript.

This work was supported by a grant from the National Institutes of Health/National Institute of Neurological Disorders and Stroke (NS 33514) to D.D. Friel.

Submitted: 2 August 2001
Revised: 22 January 2002
Accepted: 25 January 2002

REFERENCES

Akita, T., and K. Kuba. 2000. Functional triads consisting of ryanodine receptors, Ca^{2+} channels, and Ca^{2+}-activated K^+ channels in bullfrog sympathetic neurons. Plastic modulation of action potential. *J. Gen. Physiol.* 116:697–720.

Albrecht, M.A., S.L. Colegrove, J. Hongpaisan, N.B. Pivovarova, S.B. Andrews, and D.D. Friel. 2001. Multiple modes of calcium-induced calcium release in sympathetic neurons I: attenuation of endoplasmic reticulum Ca^{2+} accumulation at low $[Ca^{2+}]_i$ during weak stimulation. *J. Gen. Physiol.* 118:83–100.

Babcock, D.F., and B. Hille. 1998. Mitochondrial oversight of cellular Ca^{2+} signaling. *Curr. Opin. Neurobiol.* 8:398–404.

Baylor, S.M., W.K. Chandler, and M.W. Marshall. 1983. Sarcoplasmic reticulum calcium release in frog skeletal muscle fibers estimated from arsenazo III calcium transients. *J. Physiol.* 344:625–666.

Bergling, S., R. Dolmetsch, R.S. Lewis, and J. Keizer. 1998. A fluorometric method for estimating the calcium content of internal stores. *Cell Calcium.* 23:251–259.

Berridge, M.J. 1998. Neuronal calcium signaling. *Neuron.* 21:12–26.

Bezprozvanny, I., J. Watras, and B.E. Ehrlich. 1991. Bell-shaped calcium response curves of $Ins(1,4,5)P_3$- and calcium-gated channels from endoplasmic reticulum of cerebellum. *Nature.* 351:751–754.

Boyce, W.E., and R.C DiPrima. 1969. Elementary differential equations. John Wiley & Sons, Inc. New York. 353–357.

Clapham, D.E. 1995. Calcium signaling. *Cell.* 80:259–268.

Colegrove, S.L., M.A. Albrecht, and D.D. Friel. 2000a. Dissection of mitochondrial Ca^{2+} uptake and release fluxes after depolarization-evoked $[Ca^{2+}]_i$ elevations in sympathetic neurons. *J. Gen. Physiol.* 115:351–370.

Colegrove, S.L., M.A. Albrecht, and D.D. Friel. 2000b. Quantitative analysis of mitochondrial Ca^{2+} uptake and release pathways in sympathetic neurons: reconstruction of the recovery after depolarization-evoked $[Ca^{2+}]_i$ elevations. *J. Gen. Physiol.* 115:371–388.

Corbett, E.F., and M. Michalak. 2000. Calcium, a signaling molecule in the endoplasmic reticulum? *Trends Biochem. Sci.* 25:307–311.

East, J.M. 2000. Sarco(endo)plasmic reticulum calcium pumps: recent advances in our understanding of structure/function and biology. *Mol. Membr. Biol.* 17:189–200.

Ehrlich, B.E. 1995. Functional properties of intracellular calcium-release channels. *Curr. Opin. Neurobiol.* 5:304–309.

Friel, D.D. 1995. $[Ca^{2+}]_i$ oscillations in sympathetic neurons: an experimental test of a theoretical model. *Biophys. J.* 68:1752–1766.

Friel, D.D., and R.W. Tsien. 1992a. A caffeine- and ryanodine-sensitive Ca^{2+} store in bullfrog sympathetic neurones modulates effects of Ca^{2+} entry on $[Ca^{2+}]_i$. *J. Physiol.* 450:217–246.

Friel, D.D., and R.W. Tsien. 1992b. Phase-dependent contributions from Ca^{2+} entry and Ca^{2+} release to caffeine-induced $[Ca^{2+}]_i$ oscillations in bullfrog sympathetic neurons. *Neuron.* 8:1109–1125.

Garaschuk, O., Y. Yaari, and A. Konnerth. 1997. Release and sequestration of calcium by ryanodine-sensitive stores in rat hippocampal neurones. *J. Physiol.* 502:13–30.

Gerasimenko, O.V., J.V. Gerasimenko, A.V. Tepikin, and O.H. Petersen. 1996. Calcium transport pathways in the nucleus. *Pflügers Arch.* 432:1–6.

Hongpaisan, J., N.B. Pivovarova, S.L. Colegrove, R.D. Leapman, D.D. Friel, and S.B. Andrews. 2001. Multiple modes of calcium-induced calcium release in sympathetic neurons II: a $[Ca^{2+}]_i$-dependent transition from Ca^{2+} accumulation to net release from the endoplasmic reticulum and its spatiotemporal characteristics. *J. Gen. Physiol.* 118:101–112.

Hua, S.Y., M. Nohmi, and K. Kuba. 1993. Characteristics of Ca^{2+} release induced by Ca^{2+} influx in cultured bullfrog sympathetic neurons. *J. Physiol.* 464:245–272.

Jack, J.J.B., D. Noble, and R.W. Tsien. 1983. Electrical current flow in excitable cells. Clarendon Press, Oxford. 518 pp.

Kovacs, L., E. Rios, and M.F. Schneider. 1983. Measurement and modification of free calcium transients in frog skeletal muscle fibres by a metallochromic indicator dye. *J. Physiol.* 343:161–196.

Kuba, K. 1994. Ca^{2+}-induced Ca^{2+} release in neurons. *Jap. J. Physiol.* 44:613–650.

Kuba, K., and S. Nishi. 1976. Rhythmic hyperpolarization and depolarization of sympathetic ganglion cells induced by caffeine. *J. Neurophysiol.* 39:547–563.

Lewis, R.S. 1999. Store-operated calcium channels. *Adv. Second Messenger Phosphoprotein. Res.* 33:279–307.

Lipscombe, D., D.V. Madison, M. Poenie, H. Reuter, R.W. Tsien, and R.Y. Tsien. 1988. Imaging of cytosolic Ca^{2+} transients arising from Ca^{2+} stores and Ca^{2+} channels in sympathetic neurons. *Neuron.* 1:355–365.

Lytton, J., M. Westlin, S.E. Burk, G.E. Shull, and D.H. MacLennan. 1992. Functional comparisons between isoforms of the sarcoplasmic or endoplasmic reticulum family of calcium pumps. *J. Biol. Chem.* 267:14483–14489.

Masumiya, H., P. Li, L. Zhang, and S.R. Wayne Chen. 2001. Ryanodine sensitizes the Ca^{2+} release channel (ryanodine receptor) to Ca^{2+} activation. *J. Biol. Chem.* 276:39727–39735.

Meldolesi, J., and T. Pozzan. 1998. The endoplasmic reticulum Ca^{2+} store: a view from the lumen. *Trends Biochem. Sci.* 23:10–14.

Melzer, W., E. Rios, and M.E. Schneider. 1987. A general procedure for determining the rate of calcium release from the sarcoplasmic reticulum in skeletal muscle fibers. *Biophys. J.* 51:849–863.

Mogami, H., J. Gardner, O.V. Gerasimenko, P. Camello, O.H. Petersen, and A.V. Tepikin. 1999. Calcium binding capacity of the cytosol and endoplasmic reticulum of mouse pancreatic acinar cells. *J. Physiol.* 518:463–467.

Neher, E. 1995. The use of fura-2 for estimating Ca buffers and Ca fluxes. *Neuropharmacology.* 34:1423–1442.

Neher, E., and G.J. Augustine. 1992. Calcium gradients and buffers in bovine chromaffin cells. *J. Physiol.* 450:273–301.

Nohmi, M., S.Y. Hua, and K. Kuba. 1992. Basal Ca^{2+} and the oscillation of Ca^{2+} in caffeine-treated bullfrog sympathetic neurons. *J. Physiol.* 450:513–528.

Pivovarova, N.B., J. Hongpaisan, S.B. Andrews, and D.D. Friel. 1999. Depolarization-induced mitochondrial Ca accumulation in sympathetic neurons: spatial and temporal characteristics. *J. Neurosci.* 19:6372–6384.

Pozzan, T., R. Rizzuto, P. Volpe, and J. Meldolesi. 1994. Molecular and cellular physiology of intracellular calcium stores. *Physiol. Rev.* 74:595–636.

Rizzuto, R., P. Pinton, W. Carrington, F.S. Fay, K.E. Fogarty, L.M. Lifshitz, R.A. Tuft, and T. Pozzan. 1998. Close contacts with the endoplasmic reticulum as determinants of mitochondrial Ca^{2+} responses. *Science.* 280:1763–1766.

Rose, C.R., and A. Konnerth. 2001. Stores not just for storage: intracellular calcium release and synaptic plasticity. *Neuron.* 31:519–522.

Rousseau, E., J.S. Smith, and G. Meissner. 1987. Ryanodine modifies conductance and gating behavior of single Ca^{2+} release channel. *Am. J. Physiol.* 253:C364–C368.

Rousseau, E., J. LaDine, Q.Y. Liu, and G. Meissner. 1988. Activation of the Ca^{2+} release channel of skeletal muscle sarcoplasmic retic-

ulum by caffeine and related compounds. *Arch. Biochem. Biophys.* 267:75–86.

Sala, F., and A. Hernandez-Cruz. 1990. Calcium diffusion modeling in a spherical neuron. *Biophys. J.* 57:313–324.

Schiefer, A., G. Meissner, and G. Isenberg. 1995. Ca^{2+} activation and Ca^{2+} inactivation of canine reconstituted sarcoplasmic reticulum Ca^{2+} release channels. *J. Physiol.* 489:337–348.

Shirokova, N., A. Gonzalez, J. Ma, R. Shirodov, and E. Rios. 1995. Properties and roles of an intramembranous change mobilized at high voltages in frog skeletal muscle. *J. Physiol.* 486:385–400.

Simpson, P.B., R.A. Challiss, and S.R. Nahorski. 1995. Neuronal Ca^{2+} stores: activation and function. *Trends Neurosci.* 18:299–306.

Sipido, K.R., and W.G. Wier. 1991. Flux of Ca^{2+} across the sarcoplasmic reticulum of guinea-pig cardiac cells during excitation-contraction coupling. *J. Physiol.* 435:605–630.

Thayer, S.A., L.D. Hirning, and R.J. Miller. 1988. The role of caffeine-sensitive calcium stores in the regulation of intracellular free calcium concentration in rat sympathetic neurons in vitro. *Mol. Pharmacol.* 34:664–673.

Toescu, E.C. 1998. Intraneuronal Ca^{2+} stores act mainly as a Ca^{2+} sink; in cerebellar granule cells. *Neuroreport.* 9:1227–1231.

Tse, A., F.W. Tse, and B. Hille. 1994. Calcium homeostasis in identified rat gonadotrophs. *J. Physiol.* 477:511–525.

Usachev, Y., and S.A. Thayer. 1999. Controlling the urge for a Ca^{2+} surge: all-or-none Ca^{2+} release in neurons. *Bioessays.* 21:743–750.

Verkhratsky, A., and A. Shmigol. 1996. Calcium-induced calcium release in neurons. *Cell Calcium.* 19:1–14.

Wu, M.M., M. Grabe, S. Adams, R.Y. Tsien, H.P. Moore, and T.E. Machen. 2001. Mechanisms of pH regulation and the regulated secretory pathway. *J. Biol. Chem.* 276:33027–33035.

Xu, L., and G. Meissner. 1998. Regulation of cardiac muscle Ca^{2+} release channel by sarcoplasmic reticulum luminal Ca^{2+}. *Biophys. J.* 75:2302–2312.

Zucchi, R., and S. Roncha-Testoni. 1997. The sarcoplasmic reticulum Ca^{2+} release channel/ryanodine receptor: modulation by endogenous effectors, drugs and disease states. *Physiol. Rev.* 49:1–51.